Geochemical and isotopic (Sr-Nd-Pb) signature of crustal contamination in Na-alkali basaltic magmas of South-East Turkey

Samuele Agostini[1], Paolo Di Giuseppe[1], Piero Manetti[1,2],

Mehmet Yılmaz Savaşçın[3] & Sandro Conticelli[2,4]

[1] Istituto di Geoscienze e Georisorse, Area della Ricerca di Pisa, Consiglio Nazionale delle Ricerche, Via G. Moruzzi, 1, I-56124, Pisa, Italy.

[2] Dipartimento di Scienze della Terra, Università degli Studi di Firenze, Via G. La Pira, 4, I-50121, Firenze, Italy.

[3] Jeoloji Mühendisliği Bölümü, Munzur Üniversitesi, TR-62000, Tunceli, Turkey.

[4] Istituto di Geologia Ambientale e Geoingegneria, Consiglio Nazionale delle Ricerche, Area della Ricerca di Roma1 - Montelibretti, Via Salaria Km 29,300, 00015 Monterotondo, Italy.

S.A., 0000-0002-2060-0359; P.D.G., 0000-0002-6209-9435; S.C., 0000-0002-9204-0522.

SOCIETÀ GEOLOGICA ITALIANA
FONDATA NEL 1881 - ENTE MORALE R. D. 17 OTTOBRE 1885

ISPRA
Istituto Superiore per la Protezione e la Ricerca Ambientale

Sistema Nazionale per la Protezione dell'Ambiente

ABSTRACT

Widespread sodic alkali basaltic activity developed from Early Miocene to Pleistocene, around the northern termination of the Dead Sea Fault Zone, and in the North-West foreland of the Arabian Plate, in South-East Turkey. Volcanic activity started within the Gaziantep Basin during the Early-Late Miocene (21.2-7.0 Ma), and further East, abundant magmatism brought to the formation of the Karacadağ Shield Volcano, starting from Middle Miocene throughout the Holocene (12.1-0.01 Ma). During the Pleistocene, volcanism developed also around the Anatolia-Africa-Arabia triple junction, along the Karataş-Osmaniye Fault, and along the northern segment of the Dead Sea Fault, in the Karasu Basin.

Volcanic rocks emplaced in these areas mainly consist of abundant basalts and basanites, with subordinate hawaiites and basaltic andesites, mostly showing Na-alkaline affinity, whereas some of the older products show calc-alkaline signatures. As a whole, these volcanic rocks show LREE/HREE and HFSE/LILE ratios similar to those of OIB-like magmas. Some trace element and radiogenic isotope variations are observed amongst the less differentiated samples and they are explained by partial melting of a heterogeneous subcontinental mantle source at variable depths, mostly in the garnet stability field.

The largest compositional variability observed, however, is attributed to differentiation processes, resulting in quite remarkable chemical and isotopic variations (e.g., $^{87}Sr/^{86}Sr$ = 0.70301-0.70529; $^{143}Nd/^{144}Nd$ = 0.51263-0.51294; $^{206}Pb/^{204}Pb$ = 18.78-19.47; $^{207}Pb/^{204}Pb$ = 15.57-15.72; $^{208}Pb/^{204}Pb$ = 38.75-39.27). This implies the occurrence of open-system magma evolution, characterised by crystal fractionation at low pressure of mineral assemblage made up by olivine ± plagioclase ± clinopyroxene + apatite + Fe-Ti oxides, coupled with assimilation of crustal materials. The extent and the chemical modifications induced by this process are such that in some of the oldest and most evolved samples, the pristine Na-alkaline affinity is obliterated, and a secondary subalkaline signature is overprinted. This effect is less evident or negligible in more recent lavas, which preserve their primary features, being erupted in a well-developed fault system or in a long lasting, chemically homogeneous, magmatic feeding system.

The magmatism studied here is quite unusual and not frequent in the frame of Na-alkaline intraplate volcanism, being characterised by abundant intermediate products and by evolutionary processes strongly affected by crustal contamination. In our view, this is due to the peculiar setting of the region, which is the locus of a significant mantle upwelling, accompanied by very limited or absent extensional rate.

KEY-WORDS: Miocene-Holocene volcanism, Na-alkali basalts, assimilation plus fractional crystallisation, isotope geochemistry.

INTRODUCTION

Understanding the genesis and the origin of mafic magmas characterised by different geochemical and isotopic signatures from different tectonic settings represents an important tool to discriminate the connection between type of magmatism and tectonic evolution. In particular, Na-alkaline basaltic magmatic activity is mostly found in the oceanic islands and in within plate continental settings, as well as continental rifts. Its origin and source nature,

however, remain controversial and it is still debated. Extensive Na-alkaline lavas are also sometimes associated to strike-slip and transform faults, and strike-slip related transtensional tectonic regime, where lithospheric thinning/rupture generates magmas by decompression partial melting of sub-lithospheric and/or lithospheric mantle, or both (e.g., McKenzie & Bickle, 1988). The upraise of sub-lithospheric or lithospheric mantle causes decompression melting and generation of mafic magmas, leading to the emplacement of alkali basalts. Differently from magmas generated in oceanic islands and continental rifts, mantle-derived partial melts sourced in a within plate continental tectonic setting, as those along continental strike-slip areas, can strongly interact with upper lithospheric and crustal lithologies. Indeed, intraplate-type basaltic compositions may be modified by continental crustal assimilation combined with fractional crystallisation processes during their ascent to surface. On the other hand, pristine continental intraplate-type basalts exhibit a wide range of geochemical and isotopic compositions, which can be explained by either partial melting of (i) a depleted mantle source, retaining asthenospheric signature, or (ii) a crustal metasomatised upper mantle source with recycled continental lithosphere (e.g., Stracke et al., 2005; Rooney et al., 2014) or during magma ascent (e.g., Sparks, 1986; Kerr et al., 1995). Basaltic products erupted in these contexts, then, may be characterised by variable contents of Large Ion Lithophile Elements (LILE), Light Rare Earth Elements (LREE), High Field Strength Elements (HFSE) and radiogenic and stable isotopic compositions (e.g., Sobolev et al., 2007; Scott et al., 2016).

Most common Na-alkaline magmas erupted in continental rifts or in continental/oceanic intraplate settings are usually dominated by primitive products, along with some more evolved products with a typical bimodal distribution (e.g., Canary Islands, Wiesmaier et al., 2012; East Africa, Corti et al., 2018 and references therein). More rarely, they show a complete evolutionary trend dominated by fractional crystallisation (e.g., Azores, White et al., 1979; West Antarctica Ryft System, Rocchi et al., 2005), mostly in closed system, with negligible role played by assimilation of crustal material. Frequently, rift or intraplate magmatism may record the coexistence of limited products with transitional or sub-alkaline affinity along with predominant Na-alkaline magmas, as in the Cameroon Line (Fitton & Dunlop, 1985), Azores Island (e.g., White et al., 1979), Canary Islands (França et al., 2006) or Hyblean Plateau, Eastern Sicily (Trua et al., 1998). Magmas retaining Na-alkaline features may also form in tectonics setting characterised by low extension rate, or in transtensional basins developed along strike-slip faults, or close to triple junctions. Here, primary magmas may be affected by significant processes of source hybridisation and/or open-system evolutionary processes, with a relevant role played by interaction with crustal lithologies, sometimes resulting in a change of geochemical affinity. Given its peculiar tectonic setting, Anatolia hosts a variety of such products, from Central Anatolia (Cappadocia, Di Giuseppe et al., 2018), where a mixing trend between Na-alkaline basalts and calc-alkaline basalts can be observed, to Central-Eastern Anatolia (Sivas-Malatya, Di Giuseppe et al., 2021), in which youngest products are alkali basalts with original Na affinity, but are actually turned into K-alkali basalts due to contamination with K-rich upper crust. This is also true when considering the magmatic activity developed in Eastern Anatolia (Elazığ-Tunceli areas), where the onset of Na-alkaline activity marks the transition from compression to strike-slip tectonics (Di Giuseppe et al., 2017; Agostini et al., 2019), and at the Karlıova Triple Junction, in which both calc-alkaline products and Na-alkali basalts are found (Karaoğlu et al., 2020).

Extensive Na-alkaline intraplate-like volcanism occurred in different sectors of the Arabian Plate (Fig. 1A) at the beginning of the Late Oligocene through Pleistocene (e.g., Ilani et al., 2001; Lustrino & Sharkov, 2006; Weinstein et al., 2006; Lustrino & Wilson, 2007 and references therein). In the northern part of Arabian Plate, intracontinental basaltic volcanic activity dominated during the Late Miocene to Holocene in the Karacadağ volcanic complex (Keskin et al., 2012; Lustrino et al., 2012; Ekici et al., 2014; Nikogosian et al., 2018), and within the Şanlı Urfa and Gaziantep regions (Early-Late Miocene; Gürsoy et al., 2009; Kürüm et al., 2018). On the western border of the Arabian Plate, basaltic activity runs in South-North direction parallel to the Dead Sea Fault Zone, e.g., in the Haurun-Druze, Shin, Aleppo, Abou Ad-Dohour and Salamiyeh Plateaux (Late-Early Miocene; Lustrino & Sharkov, 2006; Krienitz et al., 2009), El-Ghab (Pleistocene; Lustrino & Sharkov, 2006) and Harrat Ash Shaam Volcanic Fields (Late Oligocene-Pleistocene; Ilani et al., 2001). To the West of the Arabian Plate, several tectonic basins with volcanic fields have developed near the Maras Triple Junction, in which Africa, Arabia, and Anatolian Plates meet (Pazarcık-Narlı, Early Miocene; Arger et al., 2000). Strike-slip related volcanic activity also occurred along the northern termination of Dead Sea Fault Zone, in the Karasu and Karataş-Osmaniye Fault Zones during the Pliocene-Pleistocene (Arger et al., 2000 and references therein; Nikogosian et al., 2018; Oyan, 2018).

Most primitive basalts in this area are the subject of a recent study, which shows the occurrence of a common mantle source, able to supply magmas with similar geochemical characteristics for long time span (>20 Ma) and in a wide region, originated by upwelling at Africa-Arabia margin, and flowing to the North-East under the Arabian plate. This mantle source retains some degree of heterogeneity, shifting between a deeper more depleted source, and shallower more enriched domain (Agostini et al., 2021). This mantle source is not only responsible for magmatism occurring in South-East Anatolia, but also for alkali basaltic rocks occurring more to the South, e.g. at Al Ghab, Homs, Aleppo, Shin Plateau and Harrat Ash Shaam (e.g., Ilani et al., 2001; Krienitz et al., 2009; Ma et al., 2011).

In this contribution, we present and discuss new geological, petrological, geochemical and isotopic data on forty-four rock samples representative of different sectors of the North-West foreland of the Arabian Plate and of the northern termination of the Dead Sea Fault Zone (Fig. 1A), integrating the data relative to eighteen less evolved samples described in Agostini et al. (2021). In particular, here, we focus our attention on the samples exhibiting some evolution degree, aiming at highlight the role of assimilation of crustal material during their uprise. Samples were collected in the Osmaniye volcanic area, in the Karasu Valley, in the Gaziantep and Şanlı Urfa regions, and in the Karacadağ Shield Volcano (Fig. 1B, C, D).

Fig. 1 - (A) Schematic tectonic and volcanological map of the Anatolian Plate and North-West Arabian Plate showing the main structural features and the areal distribution of Neogene volcanic rocks (in red); light green stars mark Maras Triple Junction (MTJ) and Karlıova Triple Junction (KTJ); NAFZ and EAFZ indicate North Anatolia Fault Zone and East Anatolia Fault Zone, respectively; BZSZ, Bitlis-Zagros Suture Zone. White boxes delimit the study areas enlarged in (B) Osmaniye and Karasu Volcanic Fields, (C) Gaziantep Volcanic Field, and (D) Karacadağ Shield Volcano. Numbers of CA- sample locations are also shown (red circles, this study; white circles, Agostini et al., 2021).

GEODYNAMIC FRAMEWORK AND REGIONAL GEOLOGY

The geodynamic evolution of the Eastern Mediterranean Region was dominated by the northward motion of African and Arabian Plates, that converged towards the Eurasian Plate since the Upper Cretaceous (e.g., Hempton, 1987; Yürür & Chorowicz, 1998). In the North the convergence induced the Neothetys Ocean to subduct along the Eurasian margin whilst at South, at the beginning of the Late Oligocene to Early Miocene, the anti-clockwise rotation of Arabian Plate led to the initial opening of Gulf of Aden, with subsequent development of the Red Sea and Suez Gulf Rift Systems (e.g., McKenzie et al., 1970; Hempton, 1987; Le Pichon & Gaulier, 1988; Shaw et al., 2003). As a response of these movements, Dead Sea Fault Zone developed as left-lateral strike-slip fault, transferring to the North the opening of Red Sea Rift and finally separating the Arabian Plate from the African ones (Le Pichon & Gaulier, 1988; Marco, 2007). The Arabia and Eurasia convergence culminated at 13 Ma (Middle Miocene) with the collision along the Bitlis-Zagros Suture Zone (BZSZ: Şengör & Yılmaz, 1981; Dewey et al., 1986; Faccenna et al., 2006; Fig. 1A). This impact gave rise to shortening and uplift in East Anatolia region (e.g., Anatolian-Iranian Plateau and Central Anatolian Plateau), the formation of the Middle Miocene North Anatolia Fault Zone (NAFZ), and the Pliocene strike-slip East Anatolia Fault Zone (EAFZ, Şengör et al., 1985; Dewey et al., 1986). In this tectonic scenario, Arabia, Africa and Anatolia meet at the Maras Triple Junction (e.g., Chorowicz et al., 1994), the connection point of the Dead Sea Fault Zone, the EAFZ and the North-East termination of the Cyprus trench (Fig. 1A). Resulting from this convergence and subsequent collision, widespread volcanism occurred in Anatolia (Eastern Anatolia and South-Eastern Anatolia), in the Anatolian-Iranian Plateau, along the Dead Sea Fault Zone, and within the northern part of the Arabian Plate. In Eastern Anatolia and throughout the Anatolian-Iranian Plateau the volcanism was mainly dominated by the emplacement of abundant products with clear subduction imprint and limited amount of volcanics showing alkaline affinities (e.g., Innocenti et al., 1982; Pearce et al., 1990; Notsu et al., 1995; Keskin et al., 1998; Di Giuseppe et al., 2017; Agostini et al., 2019; Di Giuseppe et al., 2021). On the contrary, further South, at the Anatolia-Africa-Arabia plates junction, and within the northern portion of Arabian Plate, volcanic activity resulted in the generation of mafic magmas with abundant alkali basalts, both pre-dating and post-dating the Arabia-Eurasia collision (Polat et al., 1997; Lustrino et al., 2012; Agostini et al., 2015). In more detail, volcanic products here investigated belong to the activity occurred (i) close to the strike-slip system delimited by the Karataş-Osmaniye Fault Zone (Osmanyie Volcanic Field; Fig. 1B), (ii) at the northern termination of the Dead Sea Fault Zone, called Amanos Fault Zone (Karasu Volcanic Field, Fig. 1B), and in the North-West foreland of the Arabian Plate, (iii) within the Gaziantep Basin (Fig. 1C), and (iv) in the Karacadağ Shield Volcano (Fig. 1D).

Osmanyie Volcanic Field

It is located between the Misis Range in the North-West and the Amanos Range in the East (Fig. 1B). The Misis Range represents an accretionary prism developed during the Middle Eocene-Early Miocene on the northern active margin of the southern Neotethys, and emplaced onto Miocene to Early Pliocene marine sediments (e.g., Kelling et al., 1987; Robertson et al., 2004). The Amanos Range is a portion of continental crust of the African Plate, and it is separated from Karasu Basin and Arabian Platform by the Amanos Fault (e.g., Kavak et al., 2009). The Amanos Range consists of Cretaceous ophiolites emplaced onto the Arabian Platform during the Upper Cretaceous (e.g., Dilek et al., 1999) and deep marine deposits infilled with turbiditic sediments settled during the Early Miocene, followed by deltaic sediments in the Pliocene-Quaternary time (e.g., Aksu et al., 2005). During the Pliocene to Quaternary time, left lateral strike-slip Yumurtalik and Karataş-Osmaniye fault systems developed (Fig. 1B), along which several basaltic massive lava flows were emplaced (Kelling et al., 1987; Parlak et al., 1997; Arger et al., 2000; Varol & Alpaslan, 2012; Güçtekin, 2018). These basaltic products yielded ages ranging from 2.3 to 0.12 Ma (Early-Late Pleistocene; Arger et al., 2000; Oyan, 2018), and cover Neogene sedimentary units.

Karasu Volcanic Field

The Karasu Basin is located within the EAFZ and the northern segment of the Dead Sea Fault Zone (Fig. 1B). It is characterised by Paleozoic crustal units overlapped by Mesozoic allochthonous ophiolitic complex and deformed Late Miocene-Early Pliocene sedimentary deposits (e.g., Tekeli et al., 1983; Rojay et al., 2001). In the western side, the Karasu Basin is separated from the Amanos Range by the Amanos Fault Zone, which consists of Paleozoic rocks and limbs made of Mesozoic sediments covered by ophiolitic nappes (e.g., Adiyaman & Chorowicz, 2002). Subsequently, transtensional mechanism in this sector developed in response of the EAFZ onset, as a consequence of the westward movement of the Anatolian microplate, responsible for regional extension in the Karasu Basin (Yürür & Chorowicz, 1998; Adiyaman & Chorowicz, 2002). Continental basaltic volcanism accompanied these tectonic movements, with the emplacement of alkaline basaltic products (Alıcı et al., 2001). In the southern part of the Karasu Basin, magmatism started at 1.6 Ma (Late Pleistocene), and continued in the northern part through the Middle-Late Pleistocene time (0.7-0.06 Ma; Çapan et al., 1987; Alici et al., 2001; Rojay et al., 2001).

Gaziantep Volcanic Field

West of the Amanos Range, the Gaziantep Basin mainly consists of Paleozoic and Mesozoic basement made up by shallow to deep marine sedimentary rocks and ophiolites (Coşkun & Coşkun, 2000; Alpaslan, 2007; Fig. 1C). The Tertiary units, emplaced between the Paleocene and Oligocene time, consists of shallow marine carbonates, clastic rocks and siltstones (Ulu et al., 1991; Coşkun & Coşkun, 2000). In this area, Early Miocene basalts emplaced North and South of Gaziantep Basin, around Pazarcık-Yavuzeli and Kilis towns, respectively. Here, basaltic rocks yielded age between Early Miocene to Late Miocene with the rocks outcropping around Pazarcık and Yavuzeli aged 21.2 to 12.1 Ma (Yoldemir, 1987; Gürsoy et al., 2009) and the rocks around Kilis, aged from 20.3 to 7.0 Ma (Gürsoy et al., 2009).

Karacadağ Shield Volcano

It lies South of the Arabian-Anatolian collisional zone (Fig. 1D). As reported by numerous studies, Precambrian basement made up by dacitic-rhyolitic lava sequences interlayered with pyroclastics and sandstones (Telbesemi Formation) are exposed in South-East part of the Karacadağ Shield Volcano (Keskin et al., 2012; Lustrino et al., 2012). The basement was subsequently overlapped by Cambrian formations (Sedan, Koruk and Sosink Formations) mainly composed of detrital and carbonate sediments. During the Cretaceous, these sedimentary sequences were superimposed by limestones and clay-limestones (Mardin Group and Karabogaz Formation), which are in turn overlapped by Upper Cretaceous to Paleocene clastic and carbonate rocks (Germav Formation). During the Eocene to Early Miocene time limestones were deposed on these formations (Midyat Formation; Perinçek, 1980). The Karacadağ Shield Volcano started its volcanic activity during the Late Miocene to Early Pliocene time, with basaltic rocks outcropping in its western and southern portion, belonging to the Siverek Stage (11.0-2.7 Ma; Haksal, 1981; Lustrino et al., 2010; Keskin et al., 2012; Ekici et al., 2014). Scattered lava flows belonging to the Siverek Stage outcrop also around Şanlı Urfa (Fig. 1D). Here, products span in age from 12.1 Ma (Yoldemir, 1987) to 6.65 Ma (Keskin et al., 2012).

The second volcanic phase (Karacadağ Stage) developed during the Pleistocene time (1.9-1.0 Ma) producing the main edifice of this volcanic complex (Lustrino et al., 2010; Keskin et al., 2012). The youngest products belong to the Ovabağ Stage, were emplaced during the Pleistocene-Holocene (0.4-0.01 Ma; Notsu et al., 1995; Lustrino et al., 2010; Keskin et al., 2012) and outcrop only in two limited areas in the eastern and south-eastern parts of the volcano. These last phases mainly consist of alkali basalt flows erupted from monogenetic cones (Ekici et al., 2014).

MATERIALS AND METHODS

Sixty-two (62) volcanic rocks were collected from monogenetic and composite volcanic centres from different volcanic districts of South-East Turkey. Among these, chemical and isotopic data of 18 basic samples are already available in a companion paper (Agostini et al., 2021). In data description and in the discussion, these 18 samples are merged with original data of 44 more samples presented here, including new trace element and Sr-Nd-Pb isotope data on 15 more samples, selected to be representative of most evolved samples of the region.

In more detail, nine (9) basaltic samples were collected from diverse Pleistocene lava flows, around the towns of Osmaniye and Toprakkale (Fig. 1B). Similarly, eleven (11) volcanic rocks were collected from several Pleistocene monogenetic lava flows and subordinate scoria cones, emplaced along the Amanos Fault Zone in the Karasu Volcanic Field (Fig. 1B). More to the East, we collected eight (8) volcanic rocks North of Gaziantep city, in the Pazarcık area and close to the Kırkpınar Fault Zone and minor tectonic structures, and seven (7) volcanic rocks South of Gaziantep, in the Kilis area and close to the Aafrine Fault (Fig. 1C). A total of 27 samples belonging to the Karacadağ Shield Volcano were collected. Among these, thirteen (13) lavas were sampled from the monogenetic lava flows in the Şanlı Urfa area and in the western border of Karacadağ Shield Volcano (Fig. 1D), all of them belonging to the Siverek Stage, and fourteen (14) samples were collected in different sectors of the volcano, in which both as lava flows and abundant scoria cones outcrop (11 from Karacadağ Stage, 3 from Ovabağ Stage) (Fig. 1D). Geographic details, type of rocks, GPS coordinates and petrographic features are reported in Supplementary Table 1.

Whole rock major element contents (Table 1) were determined at the Dipartimento di Scienze della Terra of the Università di Pisa by X-Ray Fluorescence (XRF). FeO content was measured via titration. Loss on Ignition (LOI) was determined by gravimetry at 1000°C after pre-heating at 110°C. Trace elements were determined on 15 selected samples by Inductively Coupled Plasma-Mass Spectrometry (ICP-MS) at Actlabs (Ontario, Canada), after lithium metaborate and lithium tetraborate fusion, according to the 4LITHO code. Analytical precision for trace elements is generally better than 5%.

Radiogenic isotopic analyses (Sr, Nd and Pb) of 15 selected samples were performed using a Thermo Fisher Neptune Plus MC-ICP-MS at the Istituto di Geoscienze e Georisorse - CNR in Pisa (Italy) in 2% HNO_3 solution containing 20-200 ng*g-1 of analyte. The instrument was equipped with a combined cyclonic and Scott-type quartz spray chamber, Ni-cones and a MicroFlow PFA 100 µl/min self-aspiring nebuliser. Rock powders were leached with strong HCl (6.6 N for half an hour at ≈ 80 °C) to cut off any effect of secondary minerals, and then rinsed 5 times with ultrapure water. Subsequently, samples were digested in a concentrated Ultrapur $HF+HNO_3$, dried and brought again into solution, then subdivided into two aliquots, one in diluted HNO_3 and one in diluted HBr. Sr was then separated from HNO_3 solution using Sr-Spec resin, Nd was separated from the same aliquot trough a two-step procedure with TRU-spec and Ln-Spec resins, whereas Pb was collected starting from the portion diluted in HBr after separation with AG50W-X8 resin.

Sr analyses were corrected for mass bias fractionation using the $^{88}Sr/^{86}Sr$ ratio (= 8.375209) and for Kr and Rb mass interferences using the ratios $^{83}Kr/^{84}Kr$ (= 0.201750), $^{83}Kr/^{86}Kr$ (= 0.664740) and $^{85}Rb/^{87}Rb$ (= 2.592310). Eight repeated analyses of standard NIST SRM 987 gave a result of 0.710348 ± 16. Results were adjusted to a ratio of 0.710248.

Instrumental mass fractionation during Nd analyses was corrected using the $^{146}Nd/^{144}Nd$ ratio (= 0.7219). Mass interference of ^{147}Sm was corrected using the ratios $^{147}Sm/^{144}Sm$ (= 4.838710), and $^{147}Sm/^{148}Sm$ (= 1.327400). Three analyses of $^{143}Nd/^{144}Nd$ ratio of reference material J-Ndi-1 gave an average of 0.512085 ± 5.

The correction for mass bias fractionation of Pb isotope ratios was performed adding a in-house Tl standard to the samples, with a $^{203}Tl/^{205}Tl$ (= 0.418882). The isobaric interferences of ^{204}Hg to ^{204}Pb was corrected using $^{202}Hg/^{204}Hg=4.35037$. During the Pb analytical set, four analyses of NIST SRM 981 standards gave following results: $^{206}Pb/^{204}Pb$= 16.9302 ± 0.0005, $^{207}Pb/^{204}Pb$=15.4848 ± 0.0005, $^{208}Pb/^{204}Pb$=36.6781 ± 0.0014. Results were normalized to values recommended by Todt et al. (1996), respectively 16.9356, 15.4891 and 36.7006 for the three isotope ratios.

Full isotope results are presented in Table 2.

Table 1 - Major and Trace Elements of studied samples

Sample	CA 72	CA 73	CA 77	CA 79	CA 93	CA 82	CA 83	CA 84	CA 85	CA 86	CA 88	CA 90	CA 91	CA 95	CA 96	CA 97	CA 98	CA 100	CA 101	CA 102
Unit	Osm	Osm	Osm	Osm	Osm	Karasu	Karasu	Karasu	Karasu	Karasu	Karasu	Karasu	Karasu	GAntep	GAntep	GAntep	GAntep	GAntep	GAntep	GAntep
Rock Type	Bsn	Bsn	A Bas	A Bas	A Bas	SA Bas	SA Bas	SA Bas	Haw	Haw	Haw	Haw	Haw	A Bas	A Bas	SA Bas	BasAnd	SA Bas	SA Bas	Haw
Major Elements (wt.%)																				
SiO_2	46.61	42.29	45.64	47.56	47.31	49.23	49.68	50.70	50.22	46.58	48.98	49.75	50.20	45.73	46.61	48.54	51.14	50.25	49.92	46.50
TiO_2	2.44	2.73	2.35	1.78	1.82	2.07	2.16	2.01	1.85	2.33	1.90	2.06	2.02	1.51	1.60	1.63	1.42	1.44	1.55	2.17
Al_2O_3	16.23	14.65	15.84	15.07	15.27	16.49	16.97	16.71	16.58	14.80	15.75	16.53	16.60	14.40	14.74	14.46	14.16	14.16	14.66	13.93
Fe_2O_3	3.24	4.90	2.49	4.02	2.05	2.72	3.22	2.80	2.58	2.49	4.81	2.88	2.58	5.43	4.22	5.59	2.67	2.78	4.12	3.19
FeO	7.34	6.13	8.72	7.73	9.52	8.36	8.53	8.24	7.84	9.15	5.98	7.74	7.90	5.75	6.45	6.06	8.20	8.01	7.40	8.07
MnO	0.17	0.15	0.15	0.16	0.15	0.15	0.16	0.15	0.14	0.16	0.14	0.15	0.14	0.14	0.14	0.15	0.14	0.14	0.18	0.15
MgO	7.44	8.83	8.92	8.46	8.30	5.94	5.17	4.95	5.59	9.01	5.68	5.48	5.60	6.72	6.33	8.52	7.57	7.50	6.92	8.38
CaO	7.62	10.33	9.86	9.43	9.62	8.76	8.86	8.47	8.40	8.76	8.35	8.16	8.42	11.13	11.90	8.19	8.66	9.17	9.06	8.77
Na_2O	5.04	4.53	3.24	3.34	2.99	3.60	3.71	3.58	3.69	3.73	3.65	3.57	3.56	3.05	3.14	3.17	2.99	3.11	3.18	3.85
K_2O	2.61	0.64	1.13	0.69	0.81	1.27	1.22	1.32	1.29	1.45	1.35	1.43	1.38	0.95	0.93	1.05	0.68	0.77	0.68	1.62
P2O5	0.63	0.59	0.37	0.37	0.30	0.43	0.32	0.29	0.45	0.59	0.60	0.40	0.37	0.32	0.28	0.34	0.19	0.21	0.22	0.49
LOI	0.60	3.23	0.60	0.67	1.09	0.78	0.63	1.20	0.61	0.85	0.59	0.91	0.78	4.21	4.26	0.91	2.12	2.50	2.26	1.93
Total	99.97	99.01	99.31	99.28	99.23	99.80	100.63	100.42	99.24	99.90	97.78	99.06	99.55	99.34	100.60	98.61	99.94	100.04	100.15	99.05
Mg#	62.15	63.80	63.12	61.06	60.57	53.62	48.76	49.18	55.46	64.16	55.50	54.56	55.36	57.06	56.51	61.77	61.78	60.01	56.72	63.42
Trace Elements (µg/g)																				
Sc						23		26			21					23	20			17
V						228		238			203					186	174			188
Cr						110		60			90					240	270			230
Co						38		34			34					51	44			48
Ni						60		30			40					190	180			210
Cu						30		20			20					60	50			60
Ga						20		20			20					19	18			21
Rb						22		20			23					21	16			19
Sr						524		350			705					428	249			662
Y						21		23			22					20	17			18
Zr						146		145			167					132	94			196
Nb						24		12			32					29	8			32
Cs											0.6						0.5			0.5
Ba						284		261			385					255	398			282
La						21.1		16			33.8					25	10.1			26.7
Ce						43.3		33.7			64.8					47.3	20.9			53.1
Pr						5.43		4.38			7.58					5.54	2.72			6.57
Nd						23.5		19.3			30.4					22.4	12.1			27.5
Sm						5.5		4.7			6.3					4.9	3.3			5.9
Eu						1.72		1.47			1.96					1.55	1.12			2.03
Gd						4.8		4.8			5.5					4.6	3.7			5.5
Tb						0.8		0.8			0.8					0.7	0.6			0.8
Dy						4.4		4.7			4.5					4.2	3.6			4.2
Ho						0.8		0.9			0.8					0.8	0.7			0.7
Er						2.3		2.5			2.2					2.2	1.8			1.8
Tm						0.31		0.35			0.3					0.31	0.24			0.22
Yb						1.8		2.1			1.8					1.8	1.5			1.3
Lu						0.3		0.32			0.29					0.29	0.24			0.18
Hf						3.3		3.5			3.6					3	2.3			4.1
Ta						1.5		0.9			1.8					1.6	0.6			2
Tl																				
Pb											6									
Th						3		2.8			4.2					3.7	1.9			3.2
U						0.5		0.6			1.1					1	0.5			0.9

Abbreviations: Osm: Osmaniye; GAntep: Gaziantep; Bsn: Basanite; A Bas: Alkali basalt; SA Bas, Subalkali Basalt; Haw, Hawaiite; BasAnd, Basaltic Andesite

Table 1 - Major and Trace Elements of studied samples *(continued)*

Sample	CA 103	CA 106	CA 107	CA 108	CA 109	CA 110	CA 113	CA 114	CA 115	CA 116	CA 117	CA 118	CA 119	CA 120	CA 121	CA 122	CA 125	CA 127	CA 128	CA 129	CA 130	CA 131	CA 132	CA 134
Unit	GAntep	GAntep	GAntep	GAntep	Osm	Siverek	Siverek	Siverek	Siverek	Siverek	Siverek	Siverek	Siverek	Siverek	Siverek	Siverek	Siverek	Siverek	Siverek	Karacadağ	Karacadağ	Karacadağ	Karacadağ	Ovabağ
Rock Type	Bsn	Bsn	A Bas	A Bas	A Bas	SA Bas	SA Bas	SA Bas	Haw	Haw	Haw	Haw	Haw	A Bas	A Bas	SA Bas	BasAnd	SA Bas	SA Bas	Haw	Bsn	Bsn	Bsn	Haw
Major Elements (wt.%)																								
SiO_2	51.33	48.72	51.37	52.59	48.59	47.04	49.06	48.66	48.81	49.55	48.62	46.16	49.91	50.15	46.82	45.85	44.99	47.85	43.81	47.21	46.05	41.97	46.06	45.83
TiO_2	1.70	1.58	1.48	1.58	2.09	2.05	1.70	1.79	1.81	1.70	1.65	2.68	2.01	2.14	2.30	2.73	1.75	2.67	2.70	3.13	3.24	4.43	3.15	2.77
Al_2O_3	14.14	13.91	14.31	14.33	13.02	13.03	14.50	14.12	14.22	14.37	14.49	13.26	15.61	15.77	13.80	13.52	14.25	14.87	13.58	16.17	17.26	14.00	17.14	13.88
Fe_2O_3	1.60	3.90	3.26	2.18	3.95	2.74	3.41	2.47	2.92	2.34	2.84	4.58	2.73	2.94	3.08	1.65	3.94	1.86	4.33	1.75	6.34	3.43	5.27	2.14
FeO	7.68	6.87	7.46	8.35	7.01	8.22	7.82	8.58	8.03	8.23	8.12	8.30	8.15	7.91	8.84	11.29	7.71	9.66	8.79	9.83	6.09	9.61	7.26	10.54
MnO	0.12	0.15	0.13	0.13	0.15	0.15	0.15	0.14	0.14	0.14	0.15	0.15	0.15	0.15	0.15	0.16	0.16	0.15	0.16	0.15	0.17	0.15	0.17	0.17
MgO	6.64	7.33	6.97	7.60	8.93	9.64	7.57	7.68	7.65	7.35	7.35	8.36	6.02	5.48	9.27	9.42	8.16	7.21	8.19	5.32	4.49	8.36	4.36	8.77
CaO	9.23	9.73	8.10	7.84	8.92	10.17	10.03	9.19	9.57	9.85	10.67	8.22	9.76	9.14	9.63	9.07	11.25	9.55	10.98	9.17	7.75	8.65	7.59	9.06
Na_2O	3.21	2.80	3.12	3.10	2.97	3.21	3.07	3.28	3.34	3.12	3.08	3.71	3.52	3.51	3.34	2.95	2.79	3.21	2.87	3.76	4.74	4.10	4.86	3.52
K_2O	1.21	0.85	0.93	0.90	1.07	1.07	0.63	0.91	0.87	0.93	0.62	1.57	0.89	0.96	1.18	0.97	0.64	1.26	0.90	1.34	2.02	2.50	2.06	1.53
P205	0.26	0.23	0.20	0.20	0.29	0.33	0.21	0.27	0.26	0.22	0.20	0.57	0.26	0.30	0.33	0.36	0.20	0.37	0.35	0.46	0.87	0.80	0.89	0.54
LOI	2.28	2.91	1.59	1.38	1.81	2.03	1.95	1.92	2.31	2.72	2.66	1.58	1.50	1.11	1.75	1.26	3.40	0.84	2.61	0.62	0.85	1.34	0.85	0.61
Total	99.40	98.98	98.92	100.18	98.80	99.67	100.10	99.01	99.93	100.51	100.46	99.14	100.50	99.56	100.49	99.23	99.24	99.50	99.27	98.91	99.87	99.34	99.65	99.37
Mg#	62.24	59.76	60.29	62.52	64.00	65.49	59.39	59.92	60.15	59.93	59.15	60.37	54.42	52.20	62.67	60.80	60.39	57.23	57.59	51.36	46.29	59.85	45.12	61.43
Trace Elements (µg/g)																								
Sc		20					23					15		22	20.9			23				15	9	21
V		183					224					215		239	239			267				327	170	261
Cr		270					330					200		200	226			230				100	<20	260
Co		47					47					52		37	59.7			43				52	31	50
Ni		210					200					200		50	221.8			100				130	20	160
Cu		70					70					60		20	44.15			50				60	20	60
Ga		18					18					25		21	23.19			21				25	26	22
Rb		15					8					18		11	17.8			13				16	15	15
Sr		340					339					858		449	503			577				1124	1091	721
Y		17					17					18		20	21.4			19				17	21	21
Zr		104					96					223		144	170.6			163				302	282	198
Nb		13					9					31		14	24.2			24				67	58	33
Cs		0.5													0.3									
Ba		505					139					348		235	213			231				342	287	214
La		12.9					10					30.6		16.9	21.1			19.4				45.4	46	29.2
Ce		26.7					21.7					63.9		35.1	45.18			41.4				90.3	91.2	60.4
Pr		3.42					2.9					8.04		4.54	5.6			5.38				10.9	10.9	7.68
Nd		15					13.1					33.9		20.2	24			23.3				43.8	44.2	32.4
Sm		3.8					3.5					7.7		4.9	5			5.6				8.7	8.7	6.9
Eu		1.34					1.29					2.61		1.73	1.7			1.86				2.8	2.85	2.32
Gd		4					3.8					6.5		4.9	5.1			5.2				6.8	7	6
Tb		0.7					0.6					0.9		0.8	0.8			0.8				0.9	1	0.9
Dy		3.7					3.7					4.7		4.5	4.7			4.4				4.6	5.3	4.9
Ho		0.7					0.7					0.8		0.8	0.9			0.8				0.7	0.9	0.9
Er		1.8					1.8					1.8		2.1	2			2				1.6	2.2	2
Tm		0.25					0.24					0.21		0.29	0.2			0.26				0.2	0.28	0.26
Yb		1.5					1.5					1.2		1.6	1.6			1.6				1.1	1.7	1.5
Lu		0.22					0.24					0.18		0.26	0.2			0.23				0.15	0.23	0.24
Hf		2.6					2.3					5.6		3.5	4.12			3.9				6.2	5.8	4.4
Ta		0.8					0.6					1.9		0.9	1.3			1.5				4	3.4	2.2
Tl		0.1																						
Pb															2.64									
Th		2					1.4					3.3		2.3	2.5			2.5				4	3.4	2.7
U		0.5					0.4					1		0.5	0.7			0.8				1.4	1.3	0.9

Abbreviations: Osm: Osmaniye; GAntep: Gaziantep; Bsn: Basanite; A Bas: Alkali basalt; SA Bas, Subalkali Basalt; Haw, Hawaiite; BasAnd, Basaltic Andesite

Table 2. Measured and age-corrected data for Sr-Nd-Pb radiogenic isotopes.

Sample	Group	Age (Ma)*	Radiogenic Isotopes					Nd Radiogenic Isotopes					Pb Radiogenic Isotopes												
			Rb	Sr	$^{87}Sr/^{86}Sr_m$	±(*10-6)	$^{87}Sr/^{86}Sr_i$	Nd	Sm	$^{143}Nd/^{144}Nd_m$	±(*10-6)	$^{143}Nd/^{144}Nd_i$	Pb	Sr	U	$^{206}Pb/^{204}Pb_m$	±	$^{207}Pb/^{204}Pb_m$	±	$^{208}Pb/^{204}Pb_m$	±	$^{206}Pb/^{204}Pb_i$	$^{207}Pb/^{204}Pb_i$	$^{208}Pb/^{204}Pb_i$
CA82	Karasu	0.78±0.10[1]	22	524	0.704252	18	**0.70425**	23.5	5.5	0.512727	9	**0.51273**	5	3.0	0.5	18.7788	0.0014	15.7159	0.0010	39.1329	0.0026	**18.779**	**15.716**	**39.133**
CA84	Karasu	0.29±0.04[2]	20	350	0.704775	9	**0.70477**	19.3	4.7	0.512692	7	**0.51269**	5	2.8	0.6	18.8814	0.0017	15.7021	0.0015	39.0241	0.0037	**18.881**	**15.702**	**39.024**
CA88	Karasu	0.45±0.15[2]	23	705	0.704187	8	**0.70419**	30.4	6.3	0.512734	5	**0.51273**	6	4.2	1.1	18.8822	0.0015	15.6987	0.0015	39.0041	0.0011	**18.882**	**15.698**	**39.004**
CA97	Gaziantep	9.22±0.2[3]	21	428	0.704523	5	**0.70450**	22.4	4.9	0.512731	4	**0.51272**	5	3.7	1.0	18.9031	0.0012	15.7188	0.0012	39.0400	0.0011	**18.903**	**15.714**	**39.038**
CA98	Gaziantep	20.27±0.05[3]	16	249	0.705340	6	**0.70529**	12.1	3.3	0.512650	6	**0.51263**	5	1.9	0.5	18.9793	0.0012	15.6435	0.0012	38.9992	0.0009	**18.979**	**15.638**	**38.997**
CA102	Gaziantep	16.32±0.01 - 18.89±0.74[3]	19	662	0.703462	5	**0.70344**	27.5	5.9	0.512852	4	**0.51284**	5	3.2	0.9	18.7821	0.0009	15.6882	0.0009	38.9203	0.0007	**18.782**	**15.679**	**38.917**
CA106	Gaziantep	16.53±0.35 - 17.74±0.40[3]	15	340	0.704429	5	**0.70440**	15.0	3.8	0.512722	6	**0.51270**	5	2.0	0.5	18.8234	0.0021	15.6714	0.0021	38.8701	0.0016	**18.823**	**15.667**	**38.868**
CA113	Siverek	10.04±0.02[3]	8	339	0.704187	6	**0.70418**	13.1	3.5	0.512782	7	**0.51277**	5	1.4	0.4	18.8234	0.0021	15.6714	0.0021	38.8701	0.0016	**18.823**	**15.669**	**38.869**
CA118	Siverek	6.65±0.35[4]	18	858	0.703627	10	**0.70362**	33.9	7.7	0.512903	6	**0.51290**	5	3.3	1.0	18.9020	0.0012	15.6273	0.0012	38.8755	0.0038	**18.902**	**15.624**	**38.874**
CA120	Siverek	6.65±0.35[4]	11	449	0.704397	8	**0.70439**	20.2	4.9	0.512742	9	**0.51274**	5	2.3	0.5	18.9389	0.0023	15.6779	0.0023	39.0648	0.0019	**18.939**	**15.676**	**39.064**
CA124	Karacadağ	3.95±0.15[4]	7	541	0.703409	6	**0.70341**	22.5	5.3	0.512874	5	**0.51287**												
CA127	Karacadağ	3.95±0.15[4]	13	577	0.703637	5	**0.70363**	23.3	5.6	0.512832	4	**0.51283**	5	2.5	0.8	19.4657	0.0068	15.6504	0.0068	39.2712	0.0052	**19.466**	**15.649**	**39.271**
CA131	Karacadağ	1.24±0.06[4]	16	1124	0.703008	4	**0.70301**	43.8	8.7	0.512944	3	**0.51294**	5	4.0	1.4	19.2258	0.0025	15.5964	0.0025	38.9357	0.0022	**19.226**	**15.595**	**38.935**
CA132	Karacadağ	1.24±0.06[4]	15	1091	0.703077	6	**0.70308**	44.2	8.7	0.512917	4	**0.51292**	5	3.4	1.3	19.2689	0.0056	15.6216	0.0056	39.0397	0.0044	**19.269**	**15.621**	**39.039**
CA134	Ovabağ	0.23±0.01[5]	15	721	0.703342	9	**0.70334**	32.4	6.9	0.512900	5	**0.51290**	5	2.7	0.9	18.9808	0.0083	15.5697	0.0083	38.7488	0.0064	**18.981**	**15.570**	**38.749**

Trace element contents in µg*g[-1]

*Age data: 1, Arger et al. (2000); 2 Rojay et al. (2001); 3 Çapan et al. (1987); 4 Alıcı et al. (2001); 5 Gursöy et al. (2009); 6 Keskin et al. (2012); 7 Notsu et al. (1995).

PETROGRAPHY

Petrographic features of the study rocks are summarised in Supplementary Table 1. The majority of the volcanic rocks are found as massive lava flows, some with vesicular texture, partially replaced by calcite filling. Subordinate scoria cones and tumulus lavas may also be locally present. All the rocks display quite similar modal composition.

Osmaniye Volcanic Field

Pleistocene basaltic rocks show sub-aphyric textures (P.I., Porphyricity Index = 1-7.5 vol.%) and contain olivine phenocrysts with subordinate clinopyroxene and plagioclase set in hypocrystalline groundmasses usually composed by abundant plagioclase and minor olivine + clinopyroxene + Fe-Ti oxides and apatite. Two samples (CA 92 and CA 93) display ophitic textures with plagioclase microphenocrysts clearly enclosed by large laths of clinopyroxene.

Karasu Volcanic Field

Pleistocene basaltic volcanic rocks emplaced in the Karasu Volcanic Field consist of subaphyric (P.I. = 2.5-7.5 vol.%) assemblage with plagioclase as most abundant phenocryst phase followed by olivine and subordinate clinopyroxene, set in hypocrystalline groundmasses made up by plagioclase, olivine, clinopyroxene, apatite and Fe-Ti oxides.

Gaziantep Volcanic Field

Early to Late Miocene basaltic rocks emplaced in the Gaziantep Basin show subaphyric (P.I. = 2.5-5 vol.%) textures, often with an ophitic character. These volcanic rocks are made of olivine, as the main phenocryst phase, with rare plagioclase set in hypocrystalline groundmasses made of plagioclase + olivine + clinopyroxene + Fe-Ti oxides + scarce apatite. Euhedral to subhedral, often skeletal, olivine shows variable degree of weathering, sometimes completely replaced by iddingsite. Secondary calcite is also commonly found in the hollow spaces between the minerals in most of the samples.

Karacadağ Shield Volcano

Middle to Late Miocene volcanic rocks from Siverek Stage are characterised by subaphyric to porphyritic (P.I. = 5-15 vol.%) to glomeroporphyric textures made of olivine and plagioclase as the main phenocryst phases followed by subordinate clinopyroxene set in hypocrystalline groundmasses made of plagioclase, olivine, clinopyroxene, apatite and Fe-Ti oxides. Two samples (CA 112 and CA 117) show hyalopilitic groundmasses. Skeletal olivine and resorbed clinopyroxene are common in the Şanlı Urfa lavas belonging to Siverek Stage. Pliocene to Holocene volcanic rocks from the Karacadağ and Ovabağ Stages show aphyric to porphyritic (P.I. = 1.5-10 vol.%) texture, with rare samples characterised by glomeroporphyritic texture. Phenocrysts consist of abundant olivine with subordinate plagioclase and clinopyroxene set in hypocrystalline groundmasses composed by plagioclase, olivine, clinopyroxene, apatite and Fe-Ti oxides.

GEOCHEMISTRY

Rock Classification

The studied rocks display a narrow range of SiO_2 (42.8-53.2 wt%, all data in this paragraph are normalised and re-calculated on a LOI-free basis) and a wide range of MgO (4.4-12.2 wt%). In the Total Alkali vs. Silica (TAS; Le Maitre, 2002) diagram they mostly plot within the basalt field with subordinate basaltic andesites, Na-trachybasalts (hawaiites), and Na-basanites/Na-tephrites, covering both alkaline and subalkaline fields (Fig. 2).
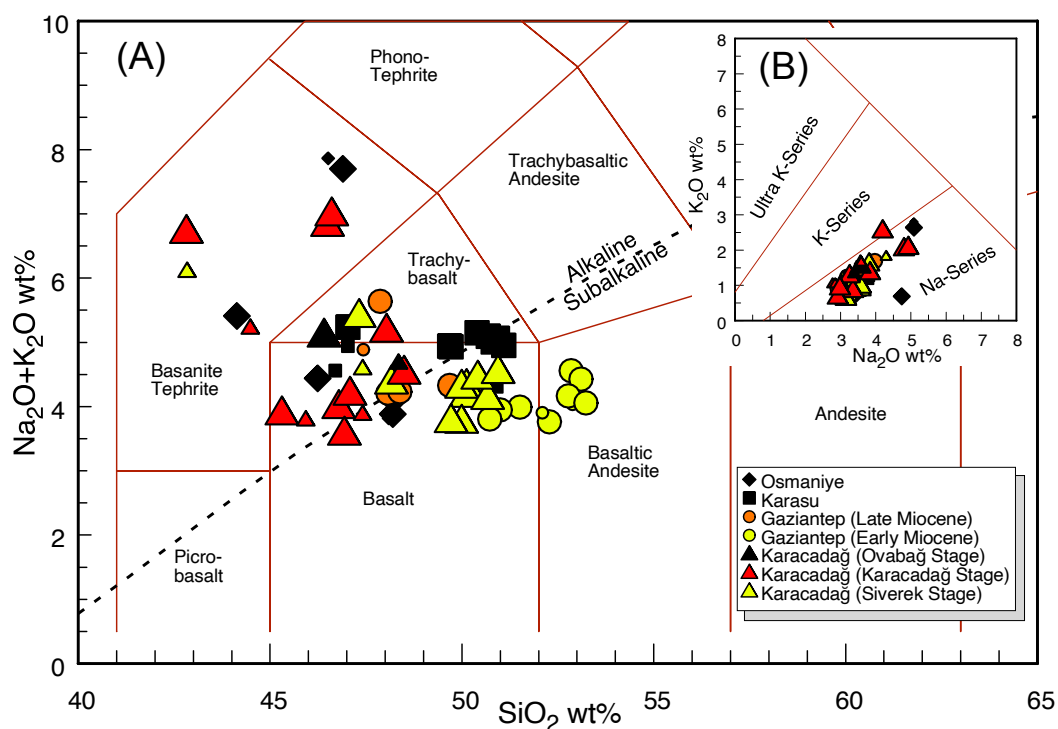
Fig. 2 - Classification diagrams for the studied rocks: (A) Total Alkali vs. Silica diagram (TAS, Le Maitre, 2002); dashed line limits the fields of the alkaline and subalkaline rocks (Irvine & Baragar, 1971); (B) K_2O vs. Na_2O diagram from Middlemost (1975). Big symbols, this study; small symbols from Agostini et al. (2021).

Osmaniye Volcanic Field

Pleistocene rocks from Osmaniye Volcanic Field are classified as basalts and basanites, they are undersaturated, *ne*-normative with a Na-alkaline character, even if four basaltic samples retain very low amounts of normative hypersthene (<3.4%; Supplementary Table 2) and two of these fall just below the alkaline-subalkaline divide line of Irvine & Baragar (1971) (Fig. 2A). On the basis of the CIPW-norm (Supplementary Table 2) these rocks range from silica-saturated (*ol-hy*-normative) to silica-undersaturated (normative ne up to 16 wt%). Using the K_2O vs. Na_2O plot (Fig. 2B), the Osmaniye rocks fall within the Na-alkaline field defined by Middlemost (1975). In addition, these rocks show a restricted range and low contents of SiO_2 (44.2-48.3 wt%), associated to high MgO contents (7.5-9.2 wt%) with Mg-# (100Mg/Mg+Fe) ranging from 60.6 to 63.8.

Karasu Volcanic Field

The volcanic rocks emplaced within the Karasu Basin are hawaiites and basalts (Fig. 2A), plotting mostly along the alkaline-subalkaline divide, with the exception of sample CA81, which fall in the subalkaline field. Karasu volcanic rocks range from Si-saturated to Si-undersaturated (normative *ne* up to 6 wt%), and according to the Middlemost's diagram are Na-alkaline. These rocks show a limited range of silica content (46.7-51.1 wt%) and wide variation of MgO content (5.0-10.0 wt%), with Mg# ranging from 48.8 to 64.2.

Gaziantep Volcanic Field

Early to Late Miocene volcanic rocks emplaced in the southern sector of the Gaziantep Basin are mostly basalts and basaltic andesites, with one sample falling in the hawaiite field. Notably, the majority of these rocks exhibit a subalkaline character (Fig. 2A), whereas the few alkali basalts and the hawaiite are Na-alkaline (Fig. 2B). It is interesting to note that even the subalkaline samples fall in the sodic field in the K_2O vs. Na_2O diagrams. As a whole, the rocks from Gaziantep Basin show the highest SiO_2 contents among the studied rocks (47.4-53.2 wt%) and a MgO varying from 6.8 to 9.1 wt%, corresponding to a Mg# ranging from 56.5 to 66.6.

Karacadağ Shield Volcano (Siverek Stage)

The majority of rocks found in Şanlı Urfa-Siverek region are subalkaline basalts, along with some alkali basalts, hawaiites and basanites (Fig. 2A). They range from silica-saturated to silica-undersaturated compositions (*ne* normative up to 16.5 wt%), and they are characterised by Na_2O-2> K_2O (Fig. 2B). The rocks emplaced in the Şanlı Urfa area show a limited range of SiO_2 (45.3-50.9 wt%), with the exception of the basanite, and wide range of variation of MgO concentrations (5.6 to 12.2 wt%) and Mg# comprised between 52.2 and 67.3.

Karacadağ Shield Volcano (Karacadağ and Ovabağ Stages)

Samples of lavas and scoriae from Karacadağ main edifice include basanites, hawaiites, and a basalt. With the exception of only one sample, which lies slightly above the sodic-potassic series line, all the samples fall in the alkaline field (Fig. 2A), and are Si-undersaturated (*ne* normative up to 15.4 wt%); hence, the rocks belonging to the Karacadağ and Ovabağ Stages are classified as Na-alkaline terms (Fig. 2B). The study rocks are characterised by a restricted variation of SiO_2 (42.8- 48.3 wt%), wide -10.2 wt%) contents and Mg# (45.1-63.2).

Major and trace element geochemistry

The major elements contents of studied samples and the trace element compositions for a subset are reported in Table 1 and, along with those analysed in Agostini et al. (2021), in Supplementary Table 2. Variations of major elements content vs. SiO_2 are plotted in Fig. 3, whereas selected trace elements vs. SiO_2 diagram are shown in Fig. 4 (A-B).

Major and trace elements

Overall, rough negative trends against SiO_2 are observed for TiO_2, FeO*, MgO and P_2O_5 (Fig. 3), whereas dispersal trend are exhibited by Al_2O_3, CaO, Na_2O and K_2O. Notably, no any major element show a clear positive correlation with SiO_2. Similar behaviour is observed for trace elements, with some elements being negatively correlated with SiO_2, and some other displaying scattered patterns. Interestingly, both some compatible elements, such as Co, V and Sr and some incompatible elements, such as Zr, La, Nb and Ta, display quite well-defined negative slopes (Fig. 4). A rough negative correlation can also be seen for Ni, Ba, Y and Th. In the following paragraph, we analyse in more detail the most significant features for the various magmatic clusters.
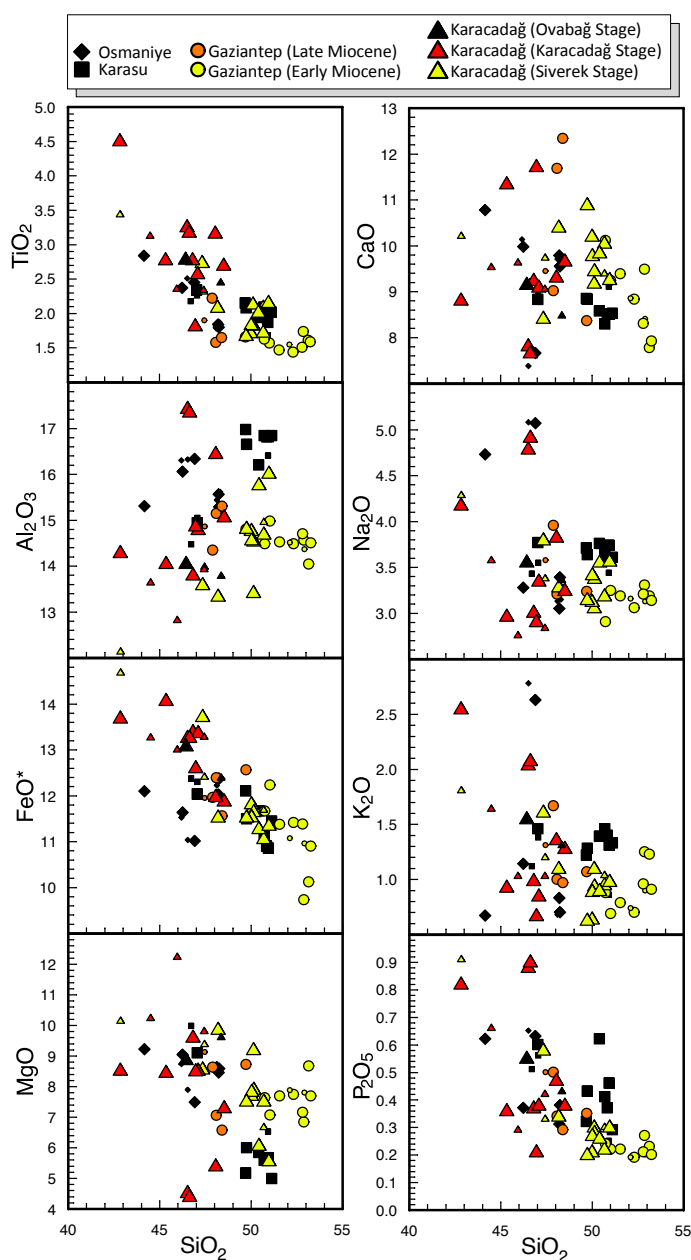
Osmaniye Volcanic Field

Pleistocene rocks from Osmaniye display low SiO_2 variation matched by high variations in some of the major elements, such as FeO*, CaO, Na_2O, K_2O, including two samples showing the highest alkali content of the studied dataset, resulting in rough vertical trends, but for MgO and TiO_2, which display negative slopes. These samples have, in general, low contents of incompatible elements, both LILE (Rb) and HFSE (Zr, Nb and Ta).

Karasu Volcanic Field

Most of the Pleistocene rocks emplaced in the Karasu Volcanic Field are easily distinguished from other studied samples for their high SiO_2 content, matched with Al_2O_3 and Na_2O enrichments, and MgO and CaO depletions. About trace elements, a negative correlation of some compatible elements (Ni, Cr and Co) can be observed, whereas V has a scattered trend.

Gaziantep Volcanic Field

Early to Late Miocene rocks from Gaziantep Volcanic Field, with respect to the other rocks of the region, exhibit quite peculiar trends. Negative correlations are observed for FeO*, CaO and, to a lesser extent Al_2O_3. MgO, as well as Na_2O, TiO_2 and P_2O_5, decrease until SiO_2 reaches $\approx$50% and then becomes flat. Notably, K_2O has a negative trend in the Late Miocene samples, that is for SiO_2<50%, and positive trend for older Early Miocene SiO_2-richer samples. Compatible trace elements split into two completely different behaviours: Ni and Cr show weak positive trends, whereas Co and V are negatively SiO_2-correlated. Interestingly, Sr is characterised by a clear negative slope, whereas incompatible elements are dispersal. Noteworthy, only in these group are present some basaltic andesites, which can be distinguished from all the other samples of the region for their very low contents of V, Sr, La, Zr, Nb and Ta.

Karacadağ Shield Volcano (Siverek Stage)

Late Miocene lavas from Şanlı Urfa region belonging to *Siverek Stage* of Karacadağ are characterised by negative correlations for TiO_2, Fe_2O_3, MgO, Na_2O, K_2O, P_2O_5, scattered CaO and positive for Al_2O_3. Most of trace elements show negative slopes, both LILE such as Ba, Rb and Sr, HFSE such as Zr, Nb, Ta as well as Th and U.

Fig. 3 - Major elements vs. SiO_2 (recalculated on a LOI-free basis) diagrams. Big symbols, this study; small symbols from Agostini et al. (2021).
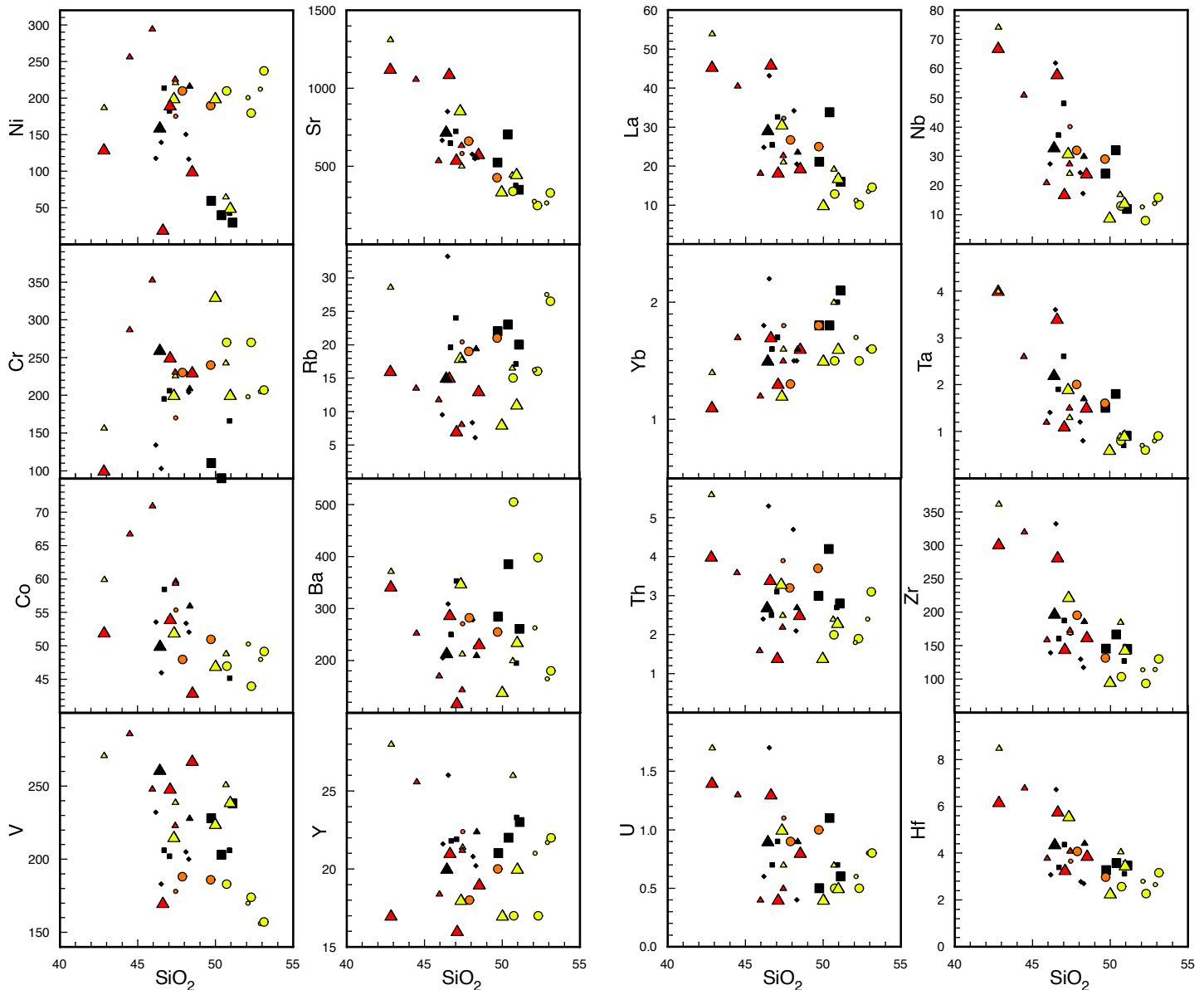
Fig. 4 - Selected trace elements vs. SiO$_2$ diagrams. Symbols as Figure 3.

Karacadağ Shield Volcano (Karacadağ and Ovabağ Stages)

Differently from what observed for the Siverek Stage, younger Pliocene-Holocene rocks belonging to the Karacadağ and Ovabağ Stages do not show clear negative correlations of major elements with SiO$_2$, rather they exhibit wide variation of most major elements combined with very small SiO$_2$ variation, resulting in vertical trends displayed in particular by FeO*, MgO, Na$_2$O and roughly positive trend for Al$_2$O$_3$. About trace elements, all the compatible ones (Ni, Co, Cr, V) as LILE (Ba, Rb and Sr), REE (La) and HFSE (such as Nb, Ta, Hf and Zr) display rough negative slopes, whereas no correlations can be seen for other elements like Th, Y or Yb.

Spider Diagrams

Primitive Mantle-normalised trace elements and Chondrite-normalised REE patterns are plotted in Fig. 5 for two older evolved samples and two younger primitive samples belonging to Gaziantep

Volcanic Field and Karacadağ Shield Volcano, respectively. Primitive magmas exhibit a humped pattern with maximum at Nb-Ta (Fig. 5A), and quite linear fractionated trend starting from most incompatible elements that are ≈50-100 times enriched with respect to Primitive Mantle, and least incompatible elements assuming values only ≈2-3 times higher than Primitive Mantle. Interestingly, older and more evolved samples have very small or no Ta-Nb positive anomaly and a much less fractionated pattern. Same trend is visible in REE patterns (Fig. 5B), where primitive samples have quite steep slopes, whereas evolved samples have more gentle trends, with an evident crossing point at Ho. None of the samples display any Eu anomaly.

Sr-Nd-Pb Isotopic Compositions

Sr-Nd-Pb isotopic compositions of the fifteen (15) selected basaltic rocks are reported in Table 2 and are plotted in Fig. 6 and Fig. 7 along with 18 samples from Agostini et al. (2021) (see also
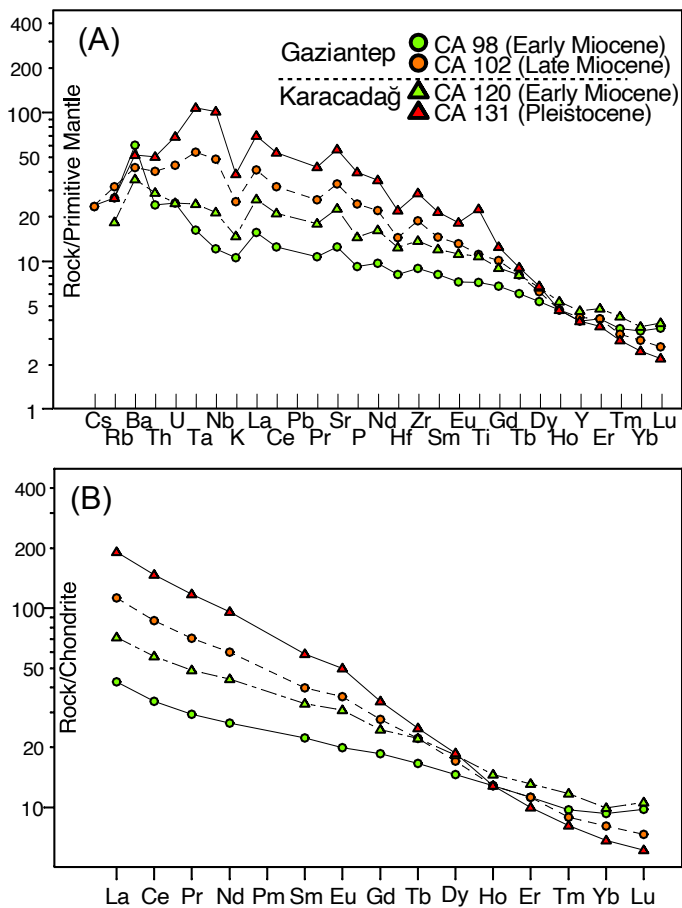
Fig. 5 - Primitive Mantle-normalised diagrams of incompatible elements (A) and Chondrite-normalised REE distribution (B) for the most primitive (CA 102 and CA 131) and the most evolved (CA 98 and CA 120) samples of Gaziantep and Karacadağ. Normalization factors from McDonough & Sun (1995).

Supplementary Table 2). Studied samples are characterised by a quite limited range of isotopic compositions varying from 0.70301-0.70529 for $^{87}Sr/^{86}Sr_{(i)}$ and 0.51263-0-51294 for $^{143}Nd/^{144}Nd_{(i)}$ isotopic ratios. As can be seen in the $^{87}Sr/^{86}Sr_{(i)}$ vs. $^{143}Nd/^{144}Nd_{(i)}$ diagram (Fig. 6), the studied rocks mostly fall in the depleted mantle quadrant within the so-called Mantle Array. However, the slope designed by Sr-Nd isotope trend of South-East Anatolia basalts does not run precisely parallel to the mantle array, retaining a shift towards more ^{87}Sr-enriched samples with respect to ^{143}Nd depletion.

It is noteworthy that most of the Pleistocene-Holocene samples (red and black symbols in Fig. 6) fall in the depleted quadrant of Fig. 6, within the FoZo-EAR (Focal Zone-European Asthenospheric Reservoir, respectively) fields, whereas the samples with highest $^{87}Sr/^{86}Sr$ values are the basaltic andesites from Gaziantep, and the sample CA 84 belonging to Karasu volcanism (along with sample CA 81 from Karasu and the sample CA 112 from Siverek Stage of Karacadağ, reported in Agostini et al., 2021): these are the most evolved rocks sampled in the study area.

The Pb isotopic data for the study rocks define a wide range of composition in Pb isotopic space. More precisely, $^{206}Pb/^{204}Pb_{(i)}$ ratio range from 18.78, to 19.47, 15.57-15.72 for the $^{207}Pb/^{204}Pb_{(i)}$

and 38.75-39.27 for $^{208}Pb/^{204}Pb_{(i)}$. Differently from the Sr-Nd isotopes, the study rocks display quite scattered variations in terms of Pb isotopes, marked by a rough negative slope in $^{207}Pb/^{204}Pb_{(i)}$ vs. $^{206}Pb/^{204}Pb_{(i)}$ (Fig. 7A), with three samples from Karacadağ Stage having $^{206}Pb/^{204}Pb$ higher than any samples reported in the literature, and with all of the samples retaining quite high $^{207}Pb/^{204}Pb$, well above the Northern Hemisphere Reference Line (NHRL, Fig. 7A) and, in general, much closer to EM-II (Enriched Mantle II) than FoZo typical values. On the contrary an almost flat trend is observed in $^{208}Pb/^{204}Pb_{(i)}$ vs. $^{206}Pb/^{204}Pb_{(i)}$ (Fig. 7B), with most of samples falling close to NHRL, well below both EM-II and FoZo, and in the same field of other alkali basalts from Western, Central and Eastern Anatolia, as well as Arabian Plate (Fig. 7B).

DISCUSSION

In the study region, volcanic activity started in the Early Miocene (21 Ma) in the North-Western sector of the Arabian foreland, within the Gaziantep Basin, with the emplacement of abundant Na-alkaline volcanic rocks and subordinate silica-oversaturated basaltic and basaltic andesitic rocks. A new pulse of Na-alkaline volcanism still in the Gaziantep Basin occurred during Middle-Late Miocene (12.1-7.0 Ma). Partially overlapping with that second pulse of magmatism, volcanism occurred in the Karacadağ area namely around Şanlı Urfa and Siverek cities (Siverek Stage; 11-2.7 Ma) with Na-alkaline lavas and subordinated silica-oversaturated basaltic rocks. Subsequently, at the end of Pliocene, through Pleistocene to Holocene, two volcanic phases (Karacadağ and Ovabağ Stages) characterised the Karacadağ Shield Volcano activity, with the production of abundant Na-alkaline magmas. Eventually, from Pleistocene to Quaternary, strike-slip related magmatism with Na-alkaline affinity developed along the northern sector of the Dead Sea Fault Zone, (e.g., Karasu Basin), and few km to the North, along the Karataş-Osmaniye strike slip fault (Osmaniye area), belonging to the Eastern Anatolia Fault Zone. Nonetheless the different eruption ages and provenance, the studied rocks share similar petrographic features, being characterised by sub-aphyric to porphyritic textures, and by a similar phenocrysts assemblage made up by olivine + plagioclase + clinopyroxene. The same phases along with apatite and Fe-Ti oxides are found in the groundmass. The occurrence of wide geochemical and isotopic variations, in a limited interval of silica content (SiO_2 = 45-55 wt%), claims for the occurrence of noteworthy differentiation processes. In the following sections, we investigate in more detail the differentiation processes discriminating those source-related from the evolution processes acting during magma ascent up to surface.

Evolution at crustal levels

Magmas showing primitive compositions are generally characterised by high values of Mg# (68-76), Ni concentrations in the range of 300-500 ppm (Frey et al., 1978) in equilibrium with mantle olivine (e.g., Fo_{91}; Albarède, 1992). In the study rocks, the abundance of phenocryst phases, as well as the wide range of MgO (4.4-12.2 wt%) and Mg# (45-67), coupled with the low and highly
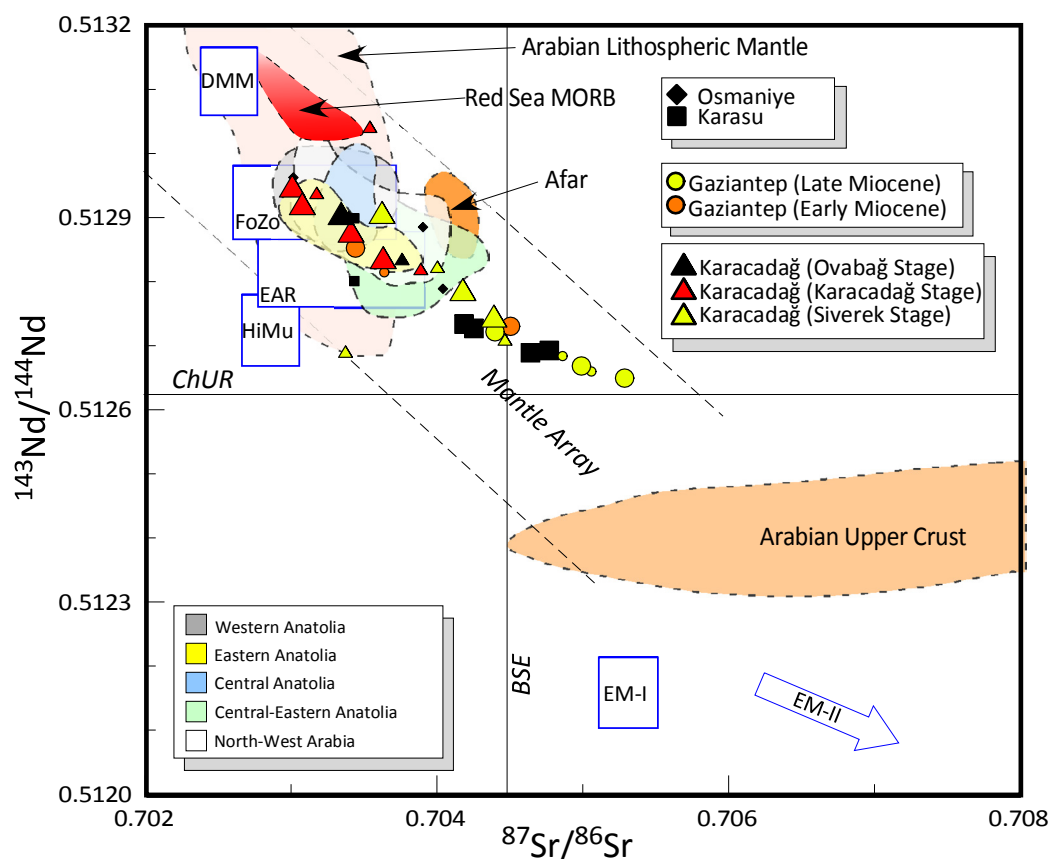
Fig. 6 - $^{143}Nd/^{144}Nd$ vs. $^{87}Sr/^{86}Sr$ isotopic ratios for the studied rocks; BSE, Bulk Silicate Earth; ChUR, Chondritic Uniform Reservoir. Mantle end-members are also reported: DMM (Depleted MORB Mantle) from Workman & Hart (2005); EAR (European Asthenospheric Reservoir) from Cebriá & Wilson (1995); FoZo (Focal Zone) from Stracke et al. (2005), HiMu = High μ (μ = $^{238}U/^{204}Pb$ ratio), EM-I (Enriched Mantle I), and EM-II (Enriched Mantle II) from Zindler & Hart (1986); Arabian Upper Crust, Arabian Lithospheric Mantle, Red Sea MORB, and Afar as in Ma et al. (2011). Fields showing the isotopic composition of primary Na-alkaline volcanic rocks of surrounding regions are from: Kula (Western Anatolia; Agostini et al., 2007), Cappadocia (Central Anatolia; Di Giuseppe et al., 2018), Sivas, Kangal and Arguvan (Central-Eastern Anatolia; Di Giuseppe et al., 2021); Elazığ (Eastern Anatolia; Di Giuseppe et al., 2017); Al Ghab-Homs, Aleppo and Shin Plateau, Harrat Ash Shaam (North-West Arabia; Lustrino & Sharkov, 2006; Krienitz et al., 2009; Ma et al., 2011). Big symbols, this study; small symbols from Agostini et al. (2021).

variable Ni concentrations (20-295 ppm) are indicative of low-pressure crystal fractionation. The overall geochemical features of the study rocks point out that magmas undergone evolutionary processes such as fractional crystallisation and/or crustal assimilation. Valuable information about fractional crystallisation and crustal assimilation, which control magma differentiation and evolution starting from a primitive composition, can be obtained through the analyses of major and trace element trends (Fig. 3 and Fig. 4). The extensive variations of MgO and Mg# values are indicative of the occurrence of significant evolution processes, mostly involving removal of femic phases from parental magmas. As a whole, the negative correlation of silica with MgO, FeO*, CaO, TiO_2 and P_2O_5 (among the major elements), and Ni, V, Co and Sr among the trace elements are indicative of a fractionation assemblage including variable proportions of olivine, clinopyroxene, Fe-Ti oxides, apatite, and plagioclase. However, the lack of any Eu anomaly (Fig. 5B), as well as the dispersal, roughly positive trend of Al_2O_3 with silica (up to $SiO_2 = 50$ wt%) suggest that plagioclase is not a dominant fractionating phase during the very first stages of magmatic differentiation (Fig. 3). The occurrence of scattered trends, however, implies that studied samples are affected also by other processes than fractional crystallisation, such as variable partial melting degree, source heterogeneity and/or evolution in open systems (Agostini et al., 2021).

On the other hand, the wide ranges of some incompatible element ratios, as well as the variations of radiogenic isotope compositions, cannot be ascribed to fractional crystallisation. In particular, since the isotopic composition is independent both from

fractional crystallisation processes, as well as the partial melting degree, increasing Sr isotopic ratios with SiO_2 is usually related with the occurrence of crustal contamination. In our dataset, wide variations of crustal-sensitive trace element ratios (e.g., Nb/U) as well as $^{87}Sr/^{86}Sr$ can be observed, and these variations are fairly correlated with SiO_2 content (Fig. 8). In particular, range of Nb/U (18-56) spans from value typical of MORBs and OiB-HiMu lavas (Nb/U > 40) in the most primitive samples, towards typical continental crust values in the relatively more evolved samples. These characteristics are indicative of digestion of crustal material during magmas ascent. To quantify the occurrence of crustal assimilation for the rocks outcropping in the study areas, Assimilation plus Fractional Crystallisation modelling (AFC; DePaolo, 1981) is performed, using the XLFRAC code (Stormer & Nicholls, 1978) and adding a contaminant among the subtracted/added phases. Here, we present (Supplementary Table 3a) different models for each volcanic suite, changing in turn starting and final composition. Lacking available published data of a local possible upper crustal assimilated material, the average upper continental crust of Rudnick & Gao (2003) was chosen as contaminant.

The occurrence of some extent of AFC is postulated for all of the various suites. However, to have a better insight on the evolutionary processes, the AFC models were both performed with or without a crustal contaminant, i.e. comparing AFC with simple FC (see Supplementary Table 3a) for Pleistocene volcanism of Osmanyie-Karasu lavas, for Early Miocene samples of Gaziantep activity, and, separately for products emitted in the older Siverek Stage and in the younger Karacadağ Stage of Karacadağ Shield Volcano.
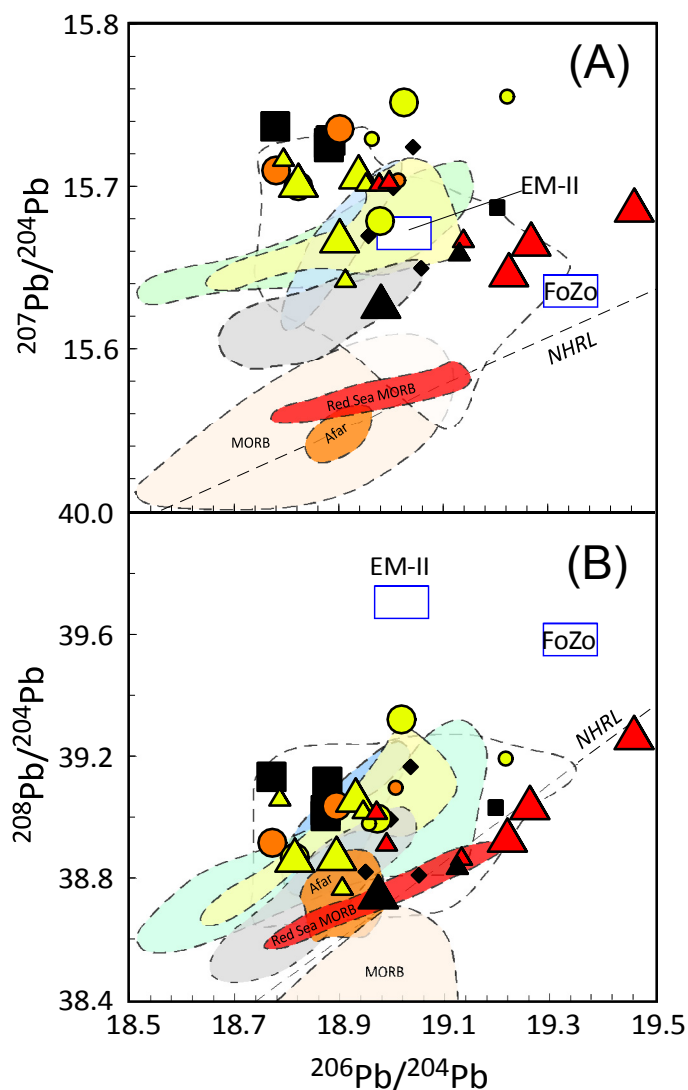
Fig. 7 - ^{207}Pb/^{204}Pb vs. ^{206}Pb/^{204}Pb and ^{208}Pb/^{204}Pb vs. ^{206}Pb/^{204}Pb diagrams. Dashed line indicates the Northern Hemisphere Reference Line (NHRL; Hart, 1984). Symbols and fields are the same of Figure 6.

Actually, for all of the suites, results with the presence of the UCC contaminant gave lower SSR (Sum of Square Residuals), and in general, the models with the presence of the UCC contaminant resulted in a lower amount of fractionated mass and in a fractionating assemblage closer to the petrographical observations.

In more detail, R is extremely low at Pleistocene Osmaniye-Karasu (Suppl. Table 3a) so that AFC and simple FC model are very close, the fractionated mass is quite high (63 to 71%) and plagioclase is the dominant phase (≈56% of fractionation assemblage).

On the contrary, Miocene lavas from Gaziantep are characterised by quite high R value (0.22), and the fractionating assemblage has plagioclase <50%. It has to be noticed that here the real contaminant should have very high ^{87}Sr/^{86}Sr isotope ratio.

Two models performed for the different stages of Karacadağ Shield Volcano are quite similar (Suppl. Table 3a). Interestingly, both models have quite high R values, which declines from 0.57 for the Late Miocene Siverek Stage to 0.32 for the Pleistocene Karacadağ

Stage. However, in agreement with the very scarce abundance of plagioclase phenocrysts, the fractionating assemblage recorded by all of the models is ultramafic and the amount of fractionated mass is limited in comparison to Osmaniye-Karasu and Gaziantep (<30%). Here, the models of simple FC, besides being unable to produce the observed shifts in trace elements and radiogenic isotope ratios (Fig. 6), are unrealistic, being characterized by high amount of plagioclase.

The results of models for the various suites were quite similar, hence we also elaborated a general model, aiming to emphasize the occurrence of a common mantle source underneath the region. Results are presented in Supplementary Tables 3b (major elements) and 3c (trace elements and isotopes), and model outputs were used to build the AFC curves presented in Fig. 8. For this model, we selected as parental magma composition the most primitive sample outcropping troughout the region, i.e. sample S92-05 from Al Ghab-Homs Volcanic Field (Western Syria, Ma et al., 2011), falling in the basanite field of TAS diagram, very close to picrobasaltic composition. The sample CA 105 from Gaziantep Volcanic Field (after Agostini et al., 2021), showing both high SiO$_2$ content, and high ^{87}Sr/^{86}Sr isotope value, was chosen as final composition.

The results of the general XLFRAC major element modelling show an Assimilation plus Fractional Crystallisation process with crystal fractionation of ≈49.5% mass removal of gabbroic assemblage made up by plagioclase (44.9%) + clinopyroxene (16.4%) + olivine (22.7%) + magnetite (12.5%) + apatite (3.5%) with ratio of assimilated mass respect to the fractionated mass (R value) of 0.40, that is indicative of digestion of 20% of crustal material. Assimilation plus Fractional Crystallisation trajectories are then calculated also for selected trace elements and radiogenic isotopes, according to the equations of DePaolo (1981), considering the same fractionation assemblage and variable degrees of R, and assuming ^{87}Sr/^{86}Sr and ^{143}Nd/^{144}Nd of contaminant, 0.713 and 0.5122, respectively (results are presented in Supplementary Table 3c). Calculated trajectories for Sr-Nd isotopes, as well as some selected trace element ratios are shown in Fig. 8. The curves match quite well the observed isotopic (Fig. 8D and G) and trace elements variations (Figs. 8A, B, C, E and F), testifying the consistency of the model, both when considering fully incompatible elements ratios (e.g., Th/Nb or Nb/U ratios, Fig. 8B and Fig. 8E), and when considering elements with different degrees of compatibility, regarding the observed mineralogical assemblage (Pl+Ol+Cpx+Mt+Ap). For instance, the significant amount of plagioclase removal causes positive slopes in Rb/Sr diagram (Fig. 8F) and negative slopes in Sr/Y diagram (Fig. 8A). However, both for radiogenic isotopes and the various trace element ratios, the curves are in general good agreement with the observed variations, considering different degrees of crustal assimilation.

Beyond the results of AFC modelling, it has to be remarked that most evolved rocks of the region are found in the Gaziantep Volcanic Field. Here, the occurrence of crustal contamination cannot only be seen from trace elements and isotope modelling, but it causes an evident change in major element compositions (Fig. 2 and Fig. 3), enough to shift these products from the alkaline to subalkaline affinity. We speculate that this is not only
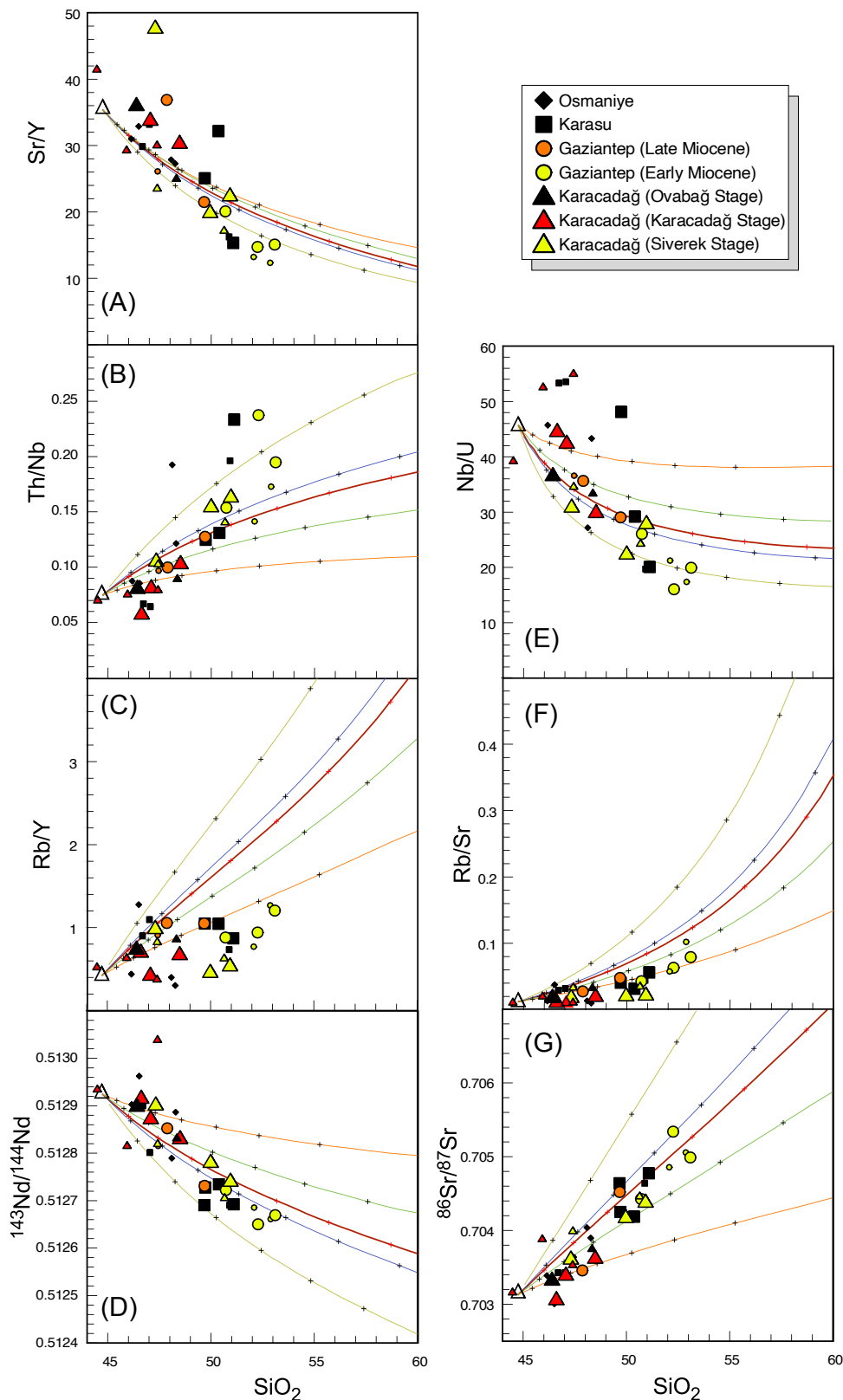
Fig. 8 - (A) Sr/Y, (B) Th/Nb, (C) Rb/Y, (D) $^{143}Nd/^{144}Nd$, (E) Nb/U, (F) Rb/Sr, (G) $^{87}Sr/^{86}Sr$ vs. SiO$_2$ diagrams showing the trajectories of the AFC (Assimilation plus Fractional Crystallisation) modelling. Calculations in Supplementary Table 3c. White triangle represents the sample chosen as representative of parental magma (sample S92-05 from Ma et al., 2011). Coloured trajectories represent different values of R; R=0.15 (orange), R=0.3 (green), R=0.4 (red), R=0.45 (blue), and R=0.6 (yellow). Crosses on the curves represent 10% steps of fractionated masses. Big symbols, this study; small symbols from Agostini et al. (2021).

due to the amount of crustal contamination, but also to a different geochemical signature of the digested material. Actually, among 15 samples collected in Gaziantep Volcanic Field, 11 are classified as subalkaline, 10 of which are actually SiO$_2$-oversaturated, and are Q-hy-normative, and only one is Ol-hy-normative. Among these, most evolved products are actually basaltic andesites, and could be classified as high-Mg andesites having SiO$_2$ of >53%, MgO of >8% on an anhydrous basis, and Mg-value (Mg#) of >60 (see Crawford et al., 1989), like the Late Miocene high-MgO andesitic belt found in Aegean-Western Anatolia (Agostini et al., 2005). However, petrography of these Gaziantep samples is not typical of high-MgO andesites or more common arc-type rocks, lacking orthopyroxene,
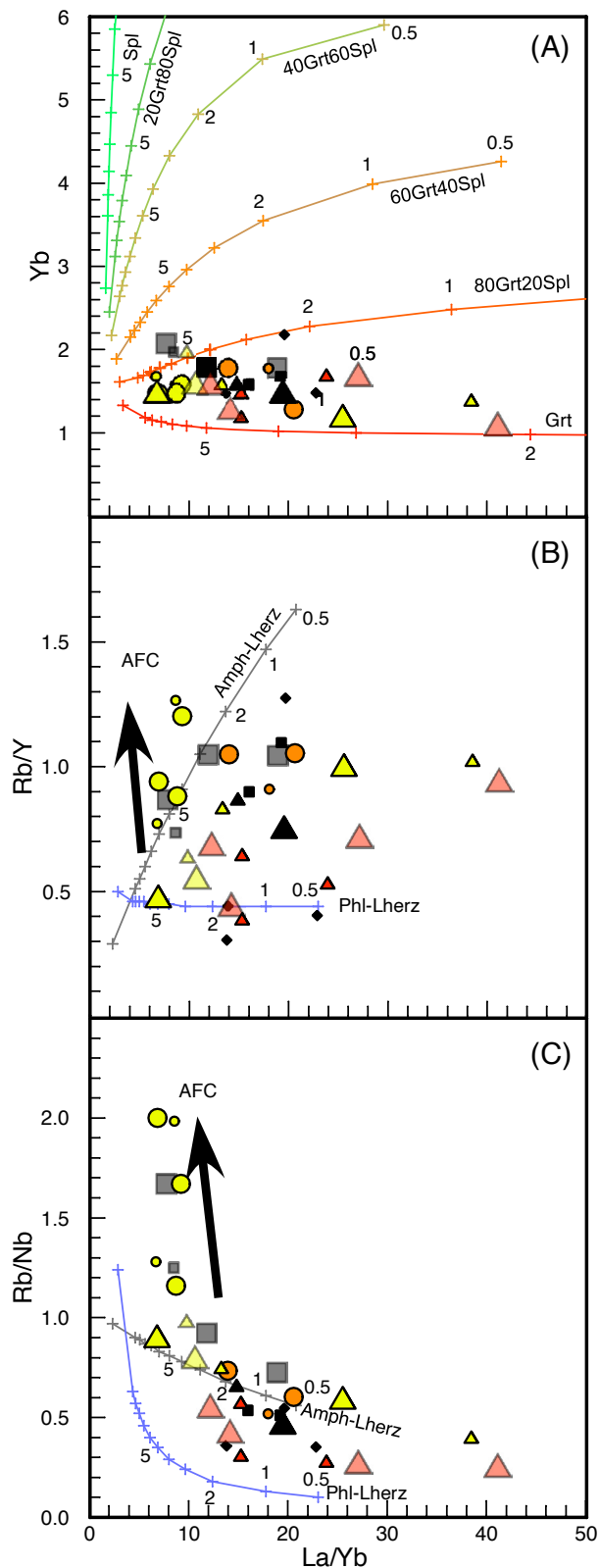
Fig. 9 - No modal batch melting trajectories for Yb vs. La/Yb diagram (A). Mineral and melt modes of spinel and garnet peridotite sources are $ol_{.578(.1)}$ + $opx_{.27(.27)}$ + $cpx_{.119(.5)}$ + $spl_{.033(.13)}$ and $ol_{.598(.05)}$ + $opx_{.211(.2)}$ + $cpx_{.076(.3)}$ + $gt_{.115(.45)}$ respectively (Thirlwall et al., 1994). Partition coefficient and Primitive Mantle compositions are reported in Supplementary Table 4; no modal batch melting trajectories for Rb/Y vs. La/Yb (B) and Rb/Nb vs. La/Yb (C) diagrams. Amphibole-bearing lherzolite and phlogopite-bearing lherzolite sources are $ol_{.550(.05)}$ + $opx_{.19(.15)}$ + $cpx_{.07(.10)}$ + $amph_{.11(.25)}$ and $ol_{.564(.17)}$ + $opx_{.188(.19)}$ + $cpx_{.141(.27)}$ + $phl_{.06(.35)}$, respectively (Witt-Eickschen et al., 1993; Duggen et al., 2005). For legend see Fig. 8. More evolved samples, i.e., those with Mg#<58, have 50% transparency (see text for explanation). Crosses on melting trajectories are at F (partial melting degree) of 0.5, 1, 2, 3, 4, 5, 6, 7, 8, 9, 10 and 20%

and retaining olivine also in groundmass. This points out for the secondary character of the calc-alkaline imprint, overprinted on the original Na-alkaline affinity of these samples, which is displayed by the less evolved samples of this volcanic field.

Spider diagrams (Fig. 5), as well as patterns of incompatible trace elements vs. SiO₂ (e.g., Rb, Ba, Y, La, Nb, Th, Ta, U; Fig 4A and Fig 4B) display some uncommon trends, which may help to have some insights on the nature of the assimilated crust. Actually, incompatible elements should have a positive correlation with SiO_2, if process is ruled by crystal fractionation, and spider diagrams of more evolved samples should display higher enrichments in the most incompatible elements, as well as steeper slopes. Studied samples have quite an opposite trend, which can only be explained if the assimilated crust is somewhat depleted in incompatible elements, so we speculate it is mostly a basic-intermediate crust.

Furthermore, it has to be noted that, both for Gaziantep Volcanic Field and Karacadağ Shield Volcano, which were active for a quite large time span, there is an evident shift from more evolved and contaminated products in the Early Miocene towards more primitive and less crustal-modified composition in Late Miocene and Pliocene. Similar trends were also observed for older basalts of Syrian plateaus (Lustrino & Sharkov, 2006). This is less evident in Osmaniye and Karasu Volcanic Fields, whose activity is restricted to Pleistocene time; in particular for Osmanyie Volcanic Field, resting on noble gases isotopes as well as other geochemical parameters, Italiano et al. (2017) exclude a significant role of continental crustal assimilation.

Finally, it has to be considered that Agostini et al. (2021) observed that some significant Sr-Nd isotope variations are found when considering only the less evolved samples, implying the occurrence of heterogeneous sources, with geochemical features varying between the depleted N-MORB type mantle and the Primitive Mantle values. In addition, the large variations occurring in major and trace elements of most primitive samples, also suggest that melting depth and melting degree vary significantly among and inside the various suites.

Magma source

The nature and heterogeneity of the magma sources of feeding volcanism in the study areas were investigated into details in a previous paper (Agostini et al. 2021), mostly combining Sr-Nd-Pb radiogenic and boron isotopes. The authors conclude that in the study area the erupted basalts reveal the occurrence of a continuous variation between a deeper and more depleted source and a shallower more enriched source, at variable depths between 100 and 60 km. In particular, they state that this mantle may have experienced some metasomatic event. However, they did not investigate into detail the role of variations of melting degree, as well as the source mineralogy, including the occurrence of hydrous phases. In the following paragraph we aim to put some constraint on these topics.

Rare Earth Element distribution may be used to evaluate the main Al-bearing phase of the mantle source and the extent of partial melting degree of the studied rock, given their variable solid/melt partition coefficients in garnet- to spinel-bearing peridotites.

To evaluate the degree of melting for the selected rocks, non-modal partial melting was simulated using the equations of Shaw (1970), and choosing the primitive mantle as starting composition (Wedepohl & Hartmann, 1994). Melting trajectories were plotted in La/Yb vs. Yb diagram (Fig. 9A). Model results, along with REE contents and partition coefficients are reported in Supplementary Table 4. Younger volcanic products belonging to the Osmaniye, Karasu, and Karacadağ (Karacadağ and Ovabağ Stages) groups are characterised by high La/Yb ratio, testifying low degree of partial melting (2-5%) in the garnet stability field, falling between the trajectory corresponding to Grt:Spl of 80:20 and 100% Grt, or very close to 100% Grt. In most cases, older rocks (*Siverek Stage* of Karacadağ and Gaziantep Volcanic Field) are characterised by lower La/Yb (6.6-13.2), indicative of higher degree of partial melting (5-10%), again between the curves of Grt:Spl of 80:20 and 100 Grt; for these samples it has also to be considered that their evolution degree may affect the La/Yb ratio, introducing a noise on this estimate.

Another open question is the eventual presence of hydrous phases in the mantle source. Previous studies on the volcanism of the North Arabian Plate invoked the occurrence of several chemically distinct components in the mantle source, as amphibole and/or phlogopite-rich veins, or a combination of the two (e.g., Polat et al., 1997; Bağci et al., 2011; Ma et al., 2011; Ekici et al., 2014; Guçtekin, 2018; Oyan, 2018). These hypotheses are also supported by the occurrence of metasomatised lithospheric mantle xenoliths, and amphibole-rich cumulate crustal xenoliths (e.g., Nasir & Safarjalani, 2000; Baker et al., 2002; Ma et al., 2011). On the other hand, these samples are characterised by a pronounced negative anomaly in Pb in the Primitive Mantle-normalised trace elements (see also Fig. 3 of Italiano et al. 2017 and Fig. 2 of Agostini et al. 2021), which can be indicative of residual amphibole and/or phlogopite in the source, given that both amphibole or phlogopite are considered to represent a main repository for Pb in the mantle (Rosenbaum, 1993). In the light of this, the relative abundances of incompatible elements can be used to evaluate the presence of hydrous phases, e.g., considering Rb/Nb and Rb/Y ratios, along with La/Yb (Fig. 9B and Fig. 9C). Rubidium was selected because it is highly compatible in phlogopite and full incompatible in amphibole, whereas Nb is more compatible in amphibole than in any other silicate mineral in melting peridotite, and Y show a moderate compatibility in amphibole, and fully incompatibility in phlogopite. Some insights can be gained observing the diagrams of Figure 9: i) rocks from Karasu, Gaziantep, and Karacadağ (Siverek and Ovabağ Stages) do not show well defined trends and some samples also shift to very high Rb/Y and Rb/Nb values due to the occurrence of variable extent of evolutionary processes (e.g., see AFC arrows in Fig. 9B and Fig. 9C). However, as a whole they plot on, or very close to, the melting curves defined for amphibole-bearing peridotite, suggesting the existence of residual amphibole in the mantle source; ii) in the rocks from Osmaniye and Karacadağ Stage of Karacadağ Shield Volcano, the role of magma evolution is negligible, hence their La/Yb, Rb/Y and Rb/Nb ratios mainly depend from mantle source character and partial melting degree. These samples exhibit evident shifts (Fig. 9B and Fig. 9C) towards residual phlogopite in their source. Results of our modelling are in agreement

with those of Oyan (2018) for Osmaniye basalts, whereas those of Güçtekin (2018) invokes amphibole bearing source also for these rocks.

In summary, the main results of mantle source modelling are as follows (temperature and pressure estimates from Agostini et al. 2021, supplementary materials).

Osmaniye Volcanic Field

Pleistocene Na-alkaline rocks from Osmaniye were segregated from their peridotitic source at approximate temperature of 1430 °C and pressure of 2.5 GPa after 2.5-4.5% of partial melting degree of garnet-bearing peridotite, suggesting that these magmas originated from phlogopite-bearing peridotitic source at depths of 60-80 km.

Karasu Volcanic Field

These rocks are characterised by magma formation occurring at higher temperatures (1450°C), but similar pressures interval (2.4 GPa) than the contemporaneous Osmaniye magmas. According to the partial melting modelling, Karasu magmas originated by 3-7% partial melting degree of garnet-bearing source, at about 70 km of depth. With respect to Osmaniye magmas, geochemical features of the Karasu magmas point out the existence of amphibole-bearing veins in their mantle source.

Gaziantep Volcanic Field

Early to Middle Miocene subalkaline magmas emplaced in the Gaziantep Basin segregated from their mantle source at segregation temperature of 1365-1415 °C and 1.3 GPa, after 7-9% of partial melting degree, with small but detectable amount of spinel (<20%, as deduced from Fig. 9A). These parameters indicate shallower depths (40 km) with respect to all of the other rocks of the study area. However, most of these rocks were subject to significant assimilation of crustal lithologies, and exhibit some degree of evolution, thus modelling results should be considered with caution. In particular, these very low depths may represent the results of re-equilibration at crustal levels during magma evolution. On the contrary, Late Miocene sample CA 94, the most primitive sample of this group, is characterised by higher segregation temperature and pressure parameters (1435 °C and 2 GPa), with degree of partial melting of 3.5% of a deeper source (70 km) in the garnet peridotite stability field, with some residual amphibole in the magma source.

Karacadağ Shield Volcano (Siverek, Karacadağ and Ovabağ Stages)

Older rocks of this shield volcano, namely the Siverek Stage, are characterised by segregation temperatures and pressures of 1460 °C and 2.0 GPa, respectively, and higher degree of partial melting (6-8%) compared to the younger Pliocene and Holocene Karacadağ and Ovabağ Stages. These ones segregated at higher temperatures of 1450-1500 °C and pressures of 2.0-3.0 GPa, after 1.5-6% partial melting degree from a deeper garnet-bearing

mantle source (64-93 km), with respect to the Siverek Stage (55-70 km). Interestingly, performed modelling show the presence of different percentage of amphibole and phlogopite in the source of the Karacadağ Shield Volcano. From one side, rocks belonging to Siverek and Ovabağ Stages indicate residual amphibole, whereas samples belonging to Karacadağ Stage the occurrence of a phlogopite-bearing mantle source.

CONCLUSIONS

In this paper, we reported new original data and genetic interpretation on basaltic activity occurred in several localities of South-East Turkey, in the North-West foreland of the Arabian Plate, and in its northwest border, close the Arabia-Africa-Anatolia triple junction.

These lavas vary in age from the Early Miocene to Pleistocene time: oldest magmas were emplaced in the Gaziantep Basin (21.2-7.0 Ma) and Karacadağ Shield Volcano (12.1-0.01 Ma), just South of the Eurasia-Arabia collisional border. More to the West, younger basaltic lava flows outcrop in the Osmaniye (2.3-0.12 Ma) and Karasu (1.6-0.06 Ma) areas, located around the Anatolia-Africa-Arabia triple junction, along the Karataş-Osmaniye Fault, and on the northern termination of the Dead Sea Fault Zone, respectively (Fig. 1).

Lavas found in Gaziantep Basin are mainly basaltic andesites with a calc-alkaline affinity. However, most primitive samples from this area are Na-alkaline, with OIB-type character. Geochemical modelling showed that the primary magmas originating these lavas were cogenetic and Na-alkaline, and that the orogenic signature of more evolved samples is a secondary feature inherited during evolutionary processes, involving significant assimilation of crustal material (e.g., high Rb/Sr, low Nb/U, high $^{87}Sr/^{86}Sr$, low $^{143}Nd/^{144}Nd$ ratio).

The Karacadağ Shield Volcano is the most prominent volcanological feature of the region and one of the biggest shield volcanoes resting on continental lithosphere, and it is constituted by Na-alkaline OIB-type products, varying in composition from basanites to hawaiites. Its activity is distinguished into three main phases, with the older magmas (Siverek Stage, 12.1-2.7 Ma) characterised by lower temperatures and pressures with respect to the younger ones (Karacadağ and Ovabağ Stages, 1.9-1.0 and 0.4-0.01 Ma). The progressive deepening of the source is paralleled by a decrease in melting degree (from ≈8% down to less than 2%), and in variable occurrences of phlogopite and amphibole in a garnet-bearing lherzolite mantle source.

The rocks outcropping close to the north-western border of Arabian Plate in the Osmaniye and Karasu Volcanic Fields span from basanites to hawaiites. They are Pleistocene in age, Na-alkaline in affinity, and show similar temperatures and pressures of primary melt segregation from a garnet-bearing mantle source, being the only remarkable difference the occurrence of dominant phlogopite (Osmaniye) or amphibole (Karasu) as hydrous phase.

As a whole, all of the primary magmas of the four investigated areas come from a garnet-bearing depleted mantle source, which is sub-continental asthenosphere subject to a passive upwelling during its eastward flow from thicker African lithosphere toward thinner Arabian lithosphere (Agostini et al. 2021). The quite wide spectrum of variations recorded in major elements, trace elements as well as radiogenic isotopes is found both considering only less evolved samples, or when considering primitive and evolved samples from the single volcanic fields. Hence, these differences (i) in part reflect primary characters of their mantle sources, which exhibit a certain degree of heterogeneity, and a progressive shift between two end members: a deep, depleted magma, characterised by low $^{87}Sr/^{86}Sr$ and high $^{143}Nd/^{144}Nd$, and a shallower, more enriched one; and (ii) in part are due to open system magma evolution, characterised by the occurrence of significant assimilation of (mafic to intermediate) crustal material and crystal fractionation at low pressure of a mineral assemblage made up by olivine ± plagioclase ± clinopyroxene + apatite + Fe-Ti oxides.

The magmatism of this region shows quite unusual characters in the frame of Na-alkaline volcanism. Indeed, these products are mostly found in areas of continental rifting or in intraplate setting, linked to upwelling of deep mantle. Commonly, Na-alkaline volcanism is restricted to basic terms (e.g. basanites to basalts and trachybasalts), or may show a typical bimodal basalt-rhyolite association, with evolution in closed system, characterised by fractional crystallization only. This is also due to the fact that most abundant Na-alkaline magmatism takes place under extensional tectonics. Here, on the contrary, we have a quite peculiar and uncommon association between a significant asthenospheric mantle uprise and a very limited or absent extensional rate. This tectonic setting creates favourable conditions for magma evolution in an open-system, with significant amount of crustal digestion, able in some case to obliterate the pristine alkaline affinity of the products. Performed models shows that this process mainly occurs in older products (Gaziantep and Siverek Stage of Karacadağ), characterised by the abundance of intermediate rocks, which exhibit a significant shift of the geochemical and isotopic imprint of these magmas, overprinting the Na-alkaline signature with a secondary calc-alkaline affinity. This effect is less evident in Pleistocene to Holocene lavas. Indeed, their emplacement in a well-developed fault system (Osmaniye and Karasu) or in a long lasting (about 20 Ma) and chemically homogeneous magmatic feeding system (Karacadağ), is able to limit the magma evolution degree, preventing the occurrence of crustal assimilation and allowing to these magmas to preserve their primary features.

ELECTRONIC SUPPLEMENTARY MATERIAL

This article contains electronic supplementary material.

ACKNOWLEDGMENTS

REFERENCES

Adiyaman Ö. & Chorowicz J. (2002) - Late Cenozoic tectonics and volcanism in the northwestern corner of the Arabian plate: a consequence of the strike-slip Dead Sea fault zone and the lateral escape of Anatolia. J. Volcanol. Geotherm. Res., 117, 327-345, https://doi.org/10.1016/S0377-0273(02)00296-2.

Agostini S., Doglioni C., Innocenti F., Manetti P., Tonarini S. & Savaşçın M.Y. (2005) - Tertiary high-Mg volcanic rocks from Western Anatolia and their geodynamic significance for the evolution of the Aegean area. In: Fytikas M. & Vougioukalakis G.E. eds., The South Aegean Active Volcanic Arc. Elsevier Book Spec Series, Develop. Volcanol., 7, 345-362, https://doi.org/10.1016/S1871-644X(05)80049-X.

Agostini S., Doglioni C., Innocenti F., Manetti P., Savaşçın M.Y. & Tonarini S. (2007) - The transition from subduction-related to intraplate Neogene magmatism in the Western Anatolia and Aegean area. In: Beccaluva L., Bianchini G. & Wilson M. eds., Cenozoic Volcanism in the Mediterranean Area. Geol. Soc. Am. Spec. Paper, 418, 1-15, https://doi.org/10.1130/2007.2418(01).

Agostini S., Manetti P., Lustrino M., Di Giuseppe P., Savaşçın M.Y. Ersoy Y. & Karaoğlu Ö. (2015) - Recent Studies on Central and Eastern Anatolia Volcanism. In: Agostini S., Manetti P. & Lustrino M. eds., The Contribution of Italian Scientists to the Geology of Turkey. Acta Volcanol., 26-27, 39-52, https://doi.org/10.19272/201500102004.

Agostini S., Savaşçın M.Y., Di Giuseppe P., Di Stefano F., Karaoğlu Ö., Lustrino M., Manetti, P., Ersoy Y., Kürüm S. & Öztufekçi Ö.A. (2019) - Neogene volcanism in Elaziğ-Tunceli area (eastern Anatolia): geocronological and petrological constraints. Ital. J. Geosci., 138, 435-455, https://doi.org/10.3301/IJG.2019.18.

Agostini S., Di Giuseppe P., Manetti P., Doglioni C. & Conticelli S. (2021) - A heterogeneous subcontinental mantle under the African–Arabian Plate boundary revealed by boron and radiogenic isotopes. Sci. Rep., 11, 11230, https://doi.org/10.1038/s41598-021-90275-7.

Aksu A., Calon T.J., Hall J. & Yaşar D. (2005) - Origin and evolution of the Neogene Iskenderum Basin, northeastern Mediterranean Sea. Mar. Geol. 221, 413-453, https://doi.org/10.1016/j.margeo.2005.03.010.

Albarède F. (1992) - How Deep Do Common Basaltic Magmas Form and Differentiate? J. Geophys. Res. 97, 10.997-11.009, https://doi.org/10.1029/91JB02927.

Alıcı P., Temel A., Gourgaud A., Vidal P. & Gündogdu M.N. (2001) - Quaternary Tholeiitic to Alkaline Volcanism in the Karasu Valley, Dead Sea Rift Zone, Southeast Turkey: Sr-Nd-Pb-O Isotopic and Trace-Element Approaches to Crust-Mantle Interaction. Int. Geol. Rev., 43, 120-138, https://doi.org/10.1080/00206810109465004.

Alpaslan M. (2007) - Early to Middle Miocene intra-continental basaltic volcanism in the northern part of the Arabian Plate, SE Anatolia, Turkey: Geochemistry and petrogenesis. Geol. Mag., 144, 867-882, https://doi.org/10.1017/S0016756807003524.

Arger J., Mitchell J. & Westaway R.W.C. (2000) - Neogene and Quaternary volcanism of southeastern Turkey. In: Bozkurt E., Winchester J.A. & Piper J.D.A. eds., Tectonics and Magmatism in Turkey and the Surrounding Area. Geol. Soc. London, Spec. Publ., 173, 459-487, https://doi.org/10.1144/GSL.SP.2000.173.01.22.

Bağci U., Alpaslan M., Frei R., Kurt M.A. & Temel A. (2011) - Different Degrees of Partial Melting of the Enriched Mantle Source for Plio-Quaternary Basic Volcanism, Toprakkale (Osmaniye) region, Southern Turkey. Turk. J. Earth Sci., 20, 115-135, https://doi.org/10.3906/yer-1003-30.

Baker J., Chazot G., Menzies M. A. & Thirlwall M. (2002) - Lithospheric mantle beneath Arabia: a Pan-African protolith modified by the Afar and older plumes, rather than a source for continental flood volcanism? In: Menzies M.A., Klemperer S.L., Ebinger C.J. & Baker J. eds., Volcanic Rifted Margins. Geol. Soc. Am. Spec. Papers, 362, 65-80, https://doi.org/10.1130/0-8137-2362-0.65.

Çapan U.Z., Vidal P. & Cantagrel L.M. (1987) - K–Ar, Nd, Sr and Pb isotopic study of Quaternary volcanism in Karasu Valley (Hatay), N-end of Dead-Sea rift zone in SE-Turkey. Yerbilimleri, 14, 165-178.

Cebriá J.M. & Wilson M. (1995) - Cenozoic mafic magmatism in Western/Central Europe: a common European asthenosphere reservoir. Terra Nova, Abs. Suppl. 7, p. 162.

Chorowicz J., Luxey P., Lyberis N., Carvalho J., Parrot J.-F., Yürür T. & Gündoğdü N. (1994) - The Maras Triple Junction (Southern Turkey) based on digital elevation model and satellite imagery interpretation. J. Geophys. Res., 99, 20225-20242, https://doi.org/10.1029/94JB00321.

Corti G., Sani F., Agostini S., Philippon M., Sokoutis D. & Willingshofer E. (2018) - Off-axis volcano-tectonic activity during continental rifting: Insights from the transversal Goba-Bonga lineament, Main Ethiopian Rift (East Africa). Tectonophysics, 728-729, 75-91, https://doi.org/10.1016/j.tecto.2018.02.011.

Coşkun H. & Coşkun B. (2000) - The Dead Sea Fault and related subsurface structures, Gaziantep Basin, southeast Turkey. Geol. Mag., 137, 175-192, htpps://doi.org/10.1017/S0016756800003770.

Crawford A.J., Falloon T.J. & Green D.H. (1989) - Classification, petrogenesis and tectonic setting of boninites. In: Crawford A.J. ed., Boninites. Unwin Hyman, London, pp. 1-49.

DePaolo D.J. (1981) - Trace element and isotopic effects of combined wallrock assimilation and fractional crystallisation. Earth Planet. Sci. Lett., 53, 189-202, https://doi.org/10.1016/0012-821X(81)90153-9.

Dewey F.J., Hempton M.R., Kidd W.S.F., Şarouğlu F. & Şengör A.M.C. (1986) - Shortening of continental lithosphere: the neotectonics of eastern Anatolia - a young collison zone. In: Coward, M.P. & Ries, A.C. eds., Collision Tectonics. Geol. Soc. London, Spec. Publ., 19, 1-36, https://doi.org/10.1144/GSL.SP.1986.019.01.01.

Di Giuseppe P., Agostini S., Lustrino M., Karaoğlu Ö., Savaşçın M.Y., Manetti P. & Ersoy Y. (2017) - Transition from Compression to Strike-slip Tectonics as Revealed by Miocene-Pleistocene Volcanism West of the Karlıova Triple Junction (East Anatolia). J. Petrol. 58(10), 2055-2087, https://doi.org/10.1093/petrology/egx082.

Di Giuseppe P., Agostini S., Savaşçın M.Y. Manetti P. & Conticelli S. (2018) - Sub-lithospheric origin of Na-alkaline and calc-alkaline magmas in a post-collisional tectonic regime: Sr-Nd-Pb isotopes in recent monogentic volcanism of Cappadocia, Central Turkey. Lithos, 316-317, 304-322, https://doi.org/10.1016/j.lithos.2018.07.018.

Di Giuseppe P., Agostini S., Di Vincenzo G., Manetti P., Savaşçın M.Y. & Conticelli S. (2021) - From subduction- to strike slip-related volcanism: insights from Sr, Nd, and Pb isotopes and geochronology of lavas from Sivas-Malatya region, Central Eastern Anatolia. Int. J. Earth Sci., 110, 849-874, https://doi.org/10.1007/s00531-021-01995-0.

Dilek Y., Thy P., Hacker B. & Grundvig S. (1999) - Structure and Petrology of Tauride ophiolites and mafic dike intrusions (Turkey): implication for the Neotethys Ocean. Geol. Soc. Am. Bull., 111, 1192-1216, https://doi.org/10.1130/0016-7606(1999)111<1192:SAPOTO>2.3.CO;2.

Duggen S., Hoernle K., Bogaard P.V.D. & Garbe-Schönberg D. (2005) - Post-collisional Transition from Subduction- to Intraplate-type Magmatism in the Westernmost Mediterranean: Evidence for Continental-edge Delamination of Subcontinental Lithosphere. J. Petrol., 46, 1155-1201, https://doi.org/10.1093/petrology/egi013.

Ekici T., Macpherson C.G., Otlu N. & Fontignie D. (2014) - Foreland Magmatism during the Arabia-Eurasia Collision: Pliocene-Quaternary Activity of the Karacadağ Volcanic Complex, SW Turkey. J. Petrol., 55, 1753-1777, https://doi.org/10.1093/petrology/egu040.

Faccenna C., Bellier O., Martinod J., Piromallo C. & Regard V. (2006) - Slab detachment beneath eastern Anatolia: A possible cause for the formation of the North Anatolian fault. Earth Planet. Sci. Lett., 242, 85-97, https://doi.org/10.1016/j.epsl.2005.11.046.

Fitton J.G. & Dunlop H.M. (1985) - The Cameroon line, West Africa, and its bearing on the origin of oceanic and continental alkali basalt. Earth Planet. Sci. Lett., 72, 23-38, https://doi.org/10.1016/0012-821X(85)90114-1.

Frey F.A., Green D. H. & Roy S.D. (1978) - Integrated Model for Basalt Petrogenesis: A Study of Quartz Tholeiites to Olivine Melilite from Southeastern Australia, Utilizing Geochemical and Experimental Petrological Data. J. Petrol. 19, 463-513, https://doi.org/10.1093/petrology/19.3.463.

França Z.T.M, Tassinari C.C.G., Cruz J.V., Aparicio A.Y., Araña V. & Rodrigues B.N. (2006) - Petrology, geochemistry and Sr−Nd−Pb isotopes of the volcanic rocks from Pico Island—Azores (Portugal). J. Volcanol. Geotherm. Res., 156, 71-89, https://doi.org/10.1016/j.jvolgeores.2006.03.013.

Güçtekin A. (2018) - Petrogenesis of Plio-Quaternary intra-plate continental alkaline lavas from the Iskenderum Gulf (Southern Turkey): Evidence for metasomatized lithospheric mantle. Chem. Erde, 78, 521-534, https://doi.org/10.1016/j.chemer.2018.08.001.

Gürsoy H., Tatar O., Piper J.D.A., Heimann A., Koçbulut F. & Mesci B.L. (2009) - Palaeomagnetic study of Tertiary volcanic domains in Southern Turkey and Neogene anticlockwise rotation of the Arabian Plate. Tectonophysics, 465, 114-127, https://doi.org/10.1016/j.tecto.2008.11.001.

Haksal A. (1981) - Petrographie und Geochemie des Schildvulkans Karacadağ, Hamburg University, Unpublished PhD Thesis.

Hart S.R. (1984) - A large-scale isotope anomaly in the southern hemisphere mantle. Nature, 309, 753-757, https://doi.org/10.1038/309753a0.

Hempton M.R. (1987) - Constraints on Arabian plate motion and extensional history of the Red Sea. Tectonics, 6, 697-705, https://doi.org/10.1029/TC006i006p00687.

Karaoğlu Ö., Gülmez F., Göçmengil G., Lustrino M., Di Giuseppe P., Manetti P., Savaşçın M.Y. & Agostini S. (2020)- Petrological evolution of Karlıova-Varto volcanism (Eastern Turkey): Magma genesis in a transtensional triple-junction tectonic setting. Lithos, 364-365, 105524, https://doi.org/10.1016/j.lithos.2020.105524.

Kavak K.S., Tatar O., Piper J., Koçbulut F. & Mesci B.L. (2009) - Determination of neotectonic features of the Karasu Basin (SE Turkey) and their relationship with Quaternary volcanic activity using Landsat ETM+imagery. Int. J. Remote Sens., 30, 4507-4524, https://doi.org/10.1080/01431160802578004.

Kelling G., Gökçen S.L., Floyd P.A. & Gökçen N. (1987) - Neogene Tectonics and Plate Convergence in the Eastern Mediterranean: New Data from Southern Turkey. Geology, 15, 425-429, https://doi.org/10.1130/0091-7613(1987)15<425:NTAPCI>2.0.CO;2.

Kerr A.C., Kempton P.D. & Thompson R.N. (1995) - Crustal assimilation during turbulent magma ascent (ATA); new isotopic evidence from the Mull Tertiary lava succession, N.W. Scotland. Contrib. Mineral. Petrol., 119, 142-154, https://doi.org/10.1007/BF00307277.

Keskin M., Pearce J.A. & Mitchell J.G. (1998) - Volcano-stratigraphy and geochemistry of collision-related volcanism on the Erzurum-Kars Plateau, North Eastern Turkey. J. Volcanol. Geotherm. Res., 85, 355-404, https://doi.org/10.1016/S0377-0273(98)00063-8.

Keskin M., Chugaev A.V., Lebedev V.A., Sharkov E.V., Oyan V. & Kavak O. (2012) - The Geochronology and Origin of Mantle Sources for Late Cenozoic Intraplate Volcanism in the Frontal Part of the Arabian Plate in the Karacadağ Neovolcanic Area of Turkey. Part 1. The Results of Isotope-Geochronological Studies. J. Volcanol. Seismol., 6, 352-360, https://doi.org/10.1134/S0742046312060036.

Krienitz M.S., Haase K.M., Mezger K., van den Bogaard P., Thiemann V. & Shaikh-Mashail M.A. (2009) - Tectonics events, continental intraplate volcanism, and mantle plume activity in northern Arabia: Contraints from geochemistry and Ar-Ar dating of Syrian lavas. Geochem. Geophys. Geosyst., 10, https://doi.org/10.1029/2008GC002254.

Kürüm S., Bölücü A. & Ural M. (2018) - Geochemistry and Petrogenesis of intracontinental Basaltic Volcanism on the Northwest Arabian Plate, Gaziantep Basin, Southeast Anatolia, Turkey. Acta Geol. Sin., 92, 519-535, https://doi.org/10.1111/1755-6724.13540.

Ilani S., Harlavan Y., Tarawneh K., Rabba I., Weinberger R., Ibrahim K., Peltz S. & Steinitz G. (2001) - New K−Ar ages of basalts from the Harrat Ash Shaam volcanic field in Jordan: Implications for the span and duration of the upper-mantle upwelling beneath the western Arabian plate. Geology, 29, 171-174, https://doi.org/10.1130/0091-7613(2001)029<0171:NKAAOB>2.0.CO;2.

Innocenti F., Mazzuoli R., Pasquarè G., Radicati di Brozolo F. & Villari L. (1982) - Tertiary and Quaternary volcanism of the Erzurum-Kars area (Eastern Turkey): Geochronological data and geodynamic evolution. J. Volcanol. Geotherm. Res., 13, 223-240, https://doi.org/10.1016/0377-0273(82)90052-X.

Irvine T.N. & Baragar W.R.A. (1971) - A guide to the chemical classification of the common volcanic rocks. Can. J. Earth Sci., 8, 523-548, https://doi.org/10.1139/e71-055.

Italiano F., Yuce G., Di Bella M., Rojay B., Sabatino G., Tripodo A., Martelli M., Rizzo A.L. & Misseri M. (2017). Noble gases and rock geochemistry of alkaline intraplate volcanics from the Amik and Ceyhan-Osmaniye areas, SE Turkey. Chem. Geol., 469, 34-46, https://doi.org/10.1016/j.chemgeo.2017.04.003.

Le Maitre R.W. (2002) - Igneous Rocks. A Classification and Glossary of Terms. Cambridge University Press, Cambridge, pp. 236, https://doi.org/10.1017/CBO9780511535581.

Le Pichon X. & Gaulier J.M. (1988) - The relation of Arabia and the Levant Fault system. Tectonophysics, 153, 271-294, https://doi.org/10.1016/0040-1951(88)90020-0.

Lustrino M. & Sharkov E. (2006) - Neogene volcanic activity of western Syria and its relationship with Arabian plate kinematics. J. Geodynam., 42, 115-139, https://doi.org/10.1016/j.jog.2006.06.003.

Lustrino M. & Wilson M. (2007) - The circum-Mediterranean anorogenic Cenozoic igneous province. Earth-Sci. Rev., 81, 1-65, https://doi.org/10.1016/j.earscirev.2006.09.002.

Lustrino M., Keskin M., Mattioli M., Lebedev V.A., Chugaev A., Sharkov E. & Kavak O. (2010) - Early activity of the largest Cenozoic shield volcano in the circum-Mediterranean area: Mt. Karacadağ, SE Turkey. Eur. J. Mineral., 22, 343-362, https://doi.org/10.1127/0935-1221/2010/0022-2024.

Lustrino M., Keskin M., Mattioli M. & Ovak O. (2012) - Heterogeneous mantle sources feeding the volcanic activity of Mt. Karacadağ (SE Turkey). J. Asian Earth Sci., 46, 120-139, https://doi.org/10.1016/j.jseaes.2011.11.016.

Ma G.S-K., Malpas J., Xenophontos C. & Chan G.H-N. (2011) - Petrogenesis of Latest Miocene-Quaternary Continental Intraplate Volcanism along the Northern Dead Sea Fault System (Al Ghab-Homs Volcanic Field), Western Syria: Evidence for Lithosphere-Asthenosphere Interaction. J. Petrol., 52, 401-430, https://doi.org/10.1093/petrology/egq085.

Marco S. (2007) - Temporal variation in the geometry of a strike-slip fault zone: Examples from the Dead Sea Transform. Tectonophysics, 445, 186-199, https://doi.org/10.1016/j.tecto.2007.08.014.

McDonough W.F. & Sun S.-s. (1995) - The composition of the Earth. Chem. Geol., 120, 223-253. https://doi.org/10.1016/0009-2541(94)00140-4.

McKenzie DP, Davis D. & Molnar P. (1970) - Plate Tectonics of the Red Sea and East Africa. Nature, 226, 243-248, https://doi.org/10.1038/226243a0.

McKenzie D. & Bickle M.J. (1988) - The Volume and Composition of Melt Generated by Extension of Lithosphere. J. Petrol., 29, 625-679, https://doi.org/10.1093/petrology/29.3.625.

Middlemost E.A.K. (1975) - The basalt clan. Earth-Sci. Rev., 11, 337-364, https://doi.org/10.1016/0012-8252(75)90039-2.

Nasir S. & Safarjalani A. (2000) - Lithospheric petrology beneath the northern part of the Arabian Plate in Syria: evidence from xenoliths in alkali basalts. J. Afr. Earth Sci., 30, 149-168, https://doi.org/10.1016/S0899-5362(00)00013-0.

Nikogosian I.K., Bracco Gartner A.J.J., van Bergen M.J., Mason P.R.D. & van Hinsbergen D.J.J. (2018) - Mantle Sources of Recent Anatolian Intraplate Magmatism: A Regional Plume or Local Tectonic Origin? Tectonics, 37, 4535-4566, htpps://doi.org.10.1029/2018TC005219.

Notsu K., Fujitani T., Ui T., Matsuda J. & Ercan T. (1995) - Geochemical features of collision-related volcanic rocks in central and eastern Anatolia, Turkey. J. Volcanol. Geotherm. Res., 64, 171-192, https://doi.org/10.1016/0377-0273(94)00077-T.

Oyan V. (2018) - Petrogenesis of the Quaternary mafic alkaline volcanism along the African-Anatolian plates boundary in Turunçlu-Delihalil (Osmaniye) region in Southern Turkey. Lithos, 314-315, 630-645, https://doi.org/10.1016/j.lithos.2018.06.008.

Parlak O., Kozlu H., Demirkol C. & Delaloye M. (1997) - Intracontinental Plio-Quaternary Volcanism along the African-Anatolian Plate Boundary, Southern Turkey. Ofioliti 22, 111-117.

Pearce J.A., Bender J.F., DeLong S.E., Kidd W.S.F., Low P.J., Güner Y., Saroğlu F., Yılmaz Y., Moorbath S. & Mitchell J.G. (1990) - Genesis of collision volcanism in Eastern Anatolia, Turkey. J. Volcanol. Geotherm. Res., 44, 189-229, https://doi.org/10.1016/0377-0273(90)90018-B.

Perinçek D. (1980) - The effects of tectonical evolution occurring in Northern Arabian Plate on the succession of the sedimentation. In: Proc. 5th Petrol. Congress, Turkey, pp. 77-93.

Polat A., Kerrich. R. & Casey J.F. (1997) - Geochemistry of Quaternary basalts erupted along the east Anatolian and Dead Sea fault zones of southern Turkey: implications for mantle sources. Lithos, 40, 55-68, https://doi.org/10.1016/S0024-4937(96)00027-8.

Robertson A., Unlügenç Ü., İnan N. & Taşlı K. (2004) - The Misis-Andırın Complex: a Mid-Tertiary Melange Related to Late-Stage Subduction of the Southern Neotethys in S Turkey. J. Asian Earth Sci., 22, 413-453, https://doi.org/10.1016/S1367-9120(03)00062-2.

Rocchi S., Armienti P. & Di Vincenzo G. (2005) - No plume, no rift magmatism in the West Antarctic Rift. In: Foulger G.R., Natland J.H., Presnall D.C. & Anderson D.L. eds., Plates, plumes, and paradigms. Geol. Soc. Am. Spec Pap., 388, 435447, https://doi.org/10.1130/0-8137-2388-4.435.

Rojay B., Heimann A. & Toprak V. (2001) - Neotectonic and volcanic characteristics of the Karasu fault zone (Anatolia, Turkey): The transition zone between the Dead Sea transform and the East Anatolian fault zone. Geodin. Acta, 14, 1-17, https://doi.org/10.1016/S0985-3111(00)01053-6.

Rooney T.O., Nelson W.R., Dosso L., Furman T. & Hanan B. (2014) - The role of continental lithosphere metasomes in the production of HIMU-like magmatism on the northeast African and Arabian plates. Geology, 42, 419-422, https://doi.org/10.1130/G35216.1.

Rosenbaum J.M. (1993) - Mantle phlogopite: a significant lead repository? Chem. Geol., 106, 475-483.

Rudnick R.L. & Gao S. (2003) - Composition of the continental crust. In: Rudnick R.L. ed., The Crust, vol. 3. Elsevier-Pergamon, Oxford, pp. 1-64, https://doi.org/10.1016/0009-2541(93)90046-L.

Scott J.M., Brenna M., Crase J.A., Waight T.E., van der Meer Q.H.A., Cooper A.F., Plain J.M., Le Roux P. & Münker C. (2016) - Peridotitic Lithosphere Metasomatized by Volatile-bearing Melts, and its Association with Intraplate Alkaline HIMU-like Magmatism. J. Petrol., 57, 2053-2078, https://doi.org/10.1093/petrology/egw069.

Şengör A.M.C. & Yılmaz Y. (1981) - Tethyan evolution of Turkey. A plate tectonic approach. Tectonophysics, 75, 181-241, https://doi.org/10.1016/0040-1951(81)90275-4.

Şengör A. M. C., Görür N. & Şaroğlu F. (1985) - Strike-slip faulting and related basin formation in zones of tectonic escape: Turkey as a case study. In: Biddle K.T. & Christie-Blick N. eds., Strike-Slip Deformation, Basin Formation, and Sedimentation. SEMP Spec. Publ., 37 (in honor of J.C. Crowell), 227- 264, https://doi.org/10.2110/pec.85.37.0211.

Shaw D. M. (1970) - Trace element fractionation during anatexis. Geochim. Cosmochim. Acta, 34, 237-243, https://doi.org/10.1016/0016-7037(70)90009-8.

Shaw J.E., Baker J.A., Menzies M.A., Thirlwall M.F. & Ibrahim K.M. (2003) - Petrogenesis of the Largest Intraplate Volcanic Field on the Arabian Plate (Jordan): a Mixed Lithosphere-Asthenosphere Source Activated by Lithospheric Extension. J. Petrol., 44, 1657-1679, https://doi.org/10.1093/petrology/egg052.

Sobolev S.V., Hofmann A.W., Kuzmin D.V., Yaxley G.M., Arndt N.T., Chung S.-L., Danyushevsky L.V., Elliott T., Frey F.A., Garcia M.O., Gurenko A.A., Kamenetsky V.S., Kerr A.C., Krivolutskaya N.A., Matvienkov V.V., Nikogosian I.K., Rocholl A., Sigurdsson I.A., Sushchevskaya N.M. & Teklay M. (2007) - The Amount of Recycled Crust in Sources of Mantle-Derived Melts. Science, 316, 412-417, https://doi.org/10.1126/science.1138113.

Sparks R.S.J. (1986) - The role of crustal contamination in magma evolution through geological time. Earth Planet. Sci. Lett., 78, 211-223, https://doi.org/10.1016/0012-821X(86)90062-2.

Stormer J.C. & Nicholls J. (1978) - XLFRAC: a program for the interactive testing of magmatic differentiation models. Comput. Geosci., 4, 143-159, https://doi.org/10.1016/0098-3004(78)90083-3.

Stracke A., Hofmann A. & Hart S.R. (2005) - FOZO, HIMU, and the rest of the mantle zoo. Geochem. Geophys. Geosyst., 6, Q05007, 7, https://doi.org/10.1029/2004GC000824.

Tekeli O., Erendil M. & Whitechurch H. (1983) - Autochtons, parautochtons and ophiolites of the Eastern Taurus and Amanos mountains. Field Guidebook (Ankara: MTA).

Thirlwall M.F., Upton B.G.J. & Jenkins C. (1994) - Interaction between Continental Lithosphere and the Iceland Plume — Sr-Nd-Pb Isotope Geochemistry of Tertiary Basalts, NE Greenland. J. Petrol., 35, 839-879, https://doi.org/10.1093/petrology/35.3.839.

Todt W., Cliff R.A., Hanser A. & Hofmann A.W. (1996) - Evaluation of a ^{202}Pb—^{205}Pb Double Spike for High - Precision Lead Isotope Analysis. In: Basu A. & Hart S. eds., Earth Processes: Reading the Isotopic Code, AGU Geophys. Monogr. Ser., 95, 429-437, https://doi.org/10.1029/GM095p0429.

Trua T., Esperança S. & Mazzuoli R. (1998) - The evolution of the lithospheric mantle along the N. African Plate: geochemical and isotopic evidence from the tholeiitic and alkaline volcanic rocks of the Hyblean plateau, Italy. Contrib. Mineral. Petrol., 131, 307-322, https://doi.org/10.1007/s004100050395.

Ulu Ü., Ercan T., Genç Ş.C., Metin Y., Çörekçioğlu E., Örçen S., Karabıyıkoğlu M., Giray S. & Yaşar T. (1991) - Geology of the Nizip-Yavuzeli-Araban-Belveren district (Gaziantep, SE Anatolia) and petrology and regional distribution of the Cenozoic volcanic rocks. Bull. Geol. Congr. Turkey, 6, 1-15.

Varol E. & Alpaslan M. (2012) - Quaternary Basaltic Volcanism Reflecting Heterogeneous Mixture of Two Mafic Melts: Gölova Basaltic Rocks, Southern Anatolia, Turkey. Geochem. Int., 50, 63-73, https://dx.doi.org/10.1134/S0016702911110097.

Wedepohl K.H. & Hartmann G. (1994) - The composition of the Primitive Upper Earth's Mantle. In: Meyer H.O.A. & Leonardos O.H. eds., Kimberlites, related rocks and mantle xenoliths. Companhia de Pesquisa de Recursos Minerais, Rio de Janeiro 1, 486-495, https://doi.org/10.29173/ikc2601.

Weinstein Y., Navon O., Altherr R. & Stein M. (2006) - The Role of Lithospheric Mantle Heterogeneity in the Generation of Plio-Pleistocene Alkali Basaltic Suites from NW Harrat Ash Shaam (Israel). J. Petrol., 47, 1017-1050, https://doi.org/10.1093/petrology/egl003.

Wiesmaier S., Troll V.R., Carracedo J.C., Ellam R.M., Bindeman I. & Wolff J.A. (2012) - Bimodality of Lavas in the Teide-Pico Viejo Succession in Tenerife-the Role of Crustal Melting in the Origin of Recent Phonolites. J. Petrol., 53, 2465-2495, https://doi.org/10.1093/petrology/egs056.

White W.M., Tapia M.D.M. & Schilling J.G. (1979) - The Petrology and Geochemistry of the Azores Islands. Contrib. Mineral. Petrol., 69, 201-213, https://doi.org/10.1007/BF00372322.

Witt-Eickschen G., Seck H.A. & Reys CH. (1993) - Multiple Enrichment Processes and their Relationships in the Subcrustal Lithosphere Beneath the Eifel (Germany). J. Petrol., 34, 1-22, https://doi.org/10.1093/petrology/34.1.1.

Workman R.K. & Hart S.R. (2005) - Major and trace element composition of the depleted MORB mantle (DMM). Earth Planet. Sci. Lett., 231, 53-72, https://doi.org/10.1016/j.epsl.2004.12.005.

Yoldemir O. (1987) - Suvarlı-Haydarlı-Narlı-Gaziantep arasında kalan alanın jeolojisi yapısal durumu ve Petrol olanakları, TPAO Rapor No: 2257, pp. 60.

Yürür M.T. & Chorowicz J. (1998) - Recent volcanism, tectonics and plate kinematics near the junction of the African, Arabian and Anatolian plates in the eastern Mediterranean. J. Volcanol. Geotherm Res., 85, 1-15, https://doi.org/10.1016/S0377-0273(98)00046-8.

Zindler A. & Hart S. (1986) - Chemical geodynamics. Ann. Rev. Earth Planet. Sci., 14, 493-571, https://doi.org/10.1146/annurev.ea.14.050186.002425.